NASA
Technical
Paper
2593

July 1986

Evaluation of Diffuse-Illumination Holographic Cinematography in a Flutter Cascade

Arthur J. Decker

NASA

NASA Technical Paper 2593

1986

Evaluation of Diffuse-Illumination Holographic Cinematography in a Flutter Cascade

Arthur J. Decker

Lewis Research Center
Cleveland, Ohio

NASA
National Aeronautics and Space Administration

Scientific and Technical Information Branch

Contents

Summary

Since 1979 the Lewis Research Center has conducted an investigation of the use of holographic cinematography for three-dimensional flow visualization. The lasers used were Q-switched, double-pulse, frequency-doubled Nd:YAG lasers, operating at 20 double-pulse per second. The primary subjects for flow visualization were the shock waves produced in two flutter cascades. The flow visualization was based on diffuse-illumination, double-exposure, holographic interferometry.

The main purpose of this investigation was to test the Nd:YAG laser, which had become a good, commercially available laboratory tool in the late 1970's, as a light source for flow-visualization holographic cinematography in wind tunnels. The interpretation of the test results involved much more than the laser performance, however. Equally important were the performances of holography and diffuse-illumination interferometry in a single-window wind tunnel and the details of the flow field itself.

The fringe-contrast factor is used to evaluate the results. That factor for an isolated flow feature is roughly the same as the hologram signal to noise. A very good hologram has a contrast factor around 100. It is argued that a practical contrast factor in a single-window wind tunnel is 10 to 20 and it is most important to eliminate specular reflections from the reconstructed images.

The effects of turbulence on shock-wave visualization in a transonic flow are discussed. It is concluded that most of the turbulent structure does not affect the fringe localization on the shock waves, but does reduce the maximum fringe contrast for shock-wave visualization.

The depth of field for visualization of a turbulent structure is demonstrated to be a measure of the relative density and scale of that structure. Hence, careful evaluation of the holograms yields properties as well as positions of flow features.

Finally, indeed, it is concluded that the Nd:YAG laser, at 5 to 50 double-exposure holograms per second, is a very effective tool for holography, if certain performance specifications are met—the most important being that the beam properties of pulses within a pulse-pair be identical.

Other items discussed in detail are the holographic emulsion, tests of coherence and polarization, effects of windows and diffusers, hologram bleaching, laser configurations, the influence and handling of specular reflections, modes of fringe localization, noise sources, and coherence requirements as a function of the pulse energy. Also, holography and diffuse illumination interferometry are reviewed.

Introduction

In 1979 a program was begun at Lewis Research Center to use the second harmonic of the Nd:YAG laser for double-exposure holography of flows. The objective was to obtain a hologram recording rate of 10 to 30 holograms per second, which was a factor of 100 to 1000 times greater than was available with a ruby laser. The purpose of this increase in recording rate was to record the time history of the geometry of a flow feature (for example, a shock-wave surface) in a periodic flow in a reasonable time. Because of its development as a holographic flow visualization method (ref. 1 to 4), diffuse-illumination, double-pulse, holographic interferometry was selected as the benchmark method for checking the holographic performance of the Nd:YAG laser. This flow visualization method, when carefully applied, yields three-dimensional images of strong flow features such as shock waves.

The Nd:YAG laser was selected for this program just as it became a commercially viable Q-switched laser (ref. 5). Its subsequent use for linear and nonlinear spectroscopy received considerable attention (refs. 6 to 8). For holography, with its own specific requirements, two configurations of the Nd:YAG laser with second-harmonic generation and a double-pulse Q-switch were investigated. Holograms of the shock waves produced in two transonic flutter cascades were recorded at a rate of 20 double-exposure holograms per second on 70-mm film. Although always useful, the holographic images were substandard.

The holograms, and the laser configurations used to record them, are discussed in the first main section of this paper. A conclusion reached in that section is that the laser design did not limit the quality of the three-dimensional shock-wave visualization in the transonic flutter cascades. Some other factor or factors in holography, interferometry, or the flow fields themselves were most influential in determining the results. To form any conclusions about the selection of a frequency-doubled Nd:YAG laser for holography at 5 to 50 double-exposure holograms per second, the influences of these nonlaser factors must be estimated. The purpose of the remainder of this paper is to provide such estimates.

First, an analysis of factors affecting hologram quality is presented. The probable cause of the holograms being substandard was light reflected from the windows and blades of the flutter cascades. Specular reflections degrade image quality for several reasons (discussed in the main section). Recording of the reflections was unavoidable because of the geometry of the holographic setup. The hologram and test section were centered and parallel, so that the shock waves could be viewed tangentially. To avoid shadowing by the blades, the angle between the object-illumination axis and the window normal was minimal. For the hologram to be close enough to the test section for three-dimensional viewing, the hologram could not avoid receiving some of the window-reflected light. The light would have been reflected away from the hologram had the angle of incidence of the object illumination been larger. An identical statement applied to the blade tips. A complicating factor was the need to admit the reference beam at a smaller angle than desired. The reason was that the 70-mm film plane was recessed about 1 cm, and it was desired to minimize shadowing of this rather small aperture. The result was that the off-axis-reference-beam criterion was not fully satisfied for the specular reflections. A solution of these problems is suggested under Results and Discussion.

Next, a similar analysis was done for diffuse-illumination interferometry as a three-dimensional visualization technique. The results of these analyses are discussed under Results and Discussion. Finally, the section, Conclusions and Concluding Remarks, contains conclusions on the selection of a Nd:YAG laser for double-exposure holographic cinematography of flows.

Laser Configurations and Performance

Two configurations of the Nd:YAG laser were used to record holograms. These configurations were TEM_{00} or stable resonator with a single-pass amplifer, and transmission-coupled unstable resonator with a single-pass amplifer. An attempt to use the stable resonator with a double-pass amplifer failed. Both configurations were operated at 20 double pulses per second.

First Configuration of the Laser System

The first configuration of the Nd:YAG laser (fig. 1) used a TEM_{00} oscillator and a single-pass amplifier. (Solid-state lasers using the stable oscillator have been described extensively in the literature (e.g., ref. 9).) The performance of this design was evaluated initially by performing single and double-exposure holography on very simple phase and reflecting objects (ref. 10). The laser performed very well in these tests, so it was transferred to a flutter cascade for evaluation in holographic flow visualization.

A typical flutter cascade (fig. 2) is a wind tunnel containing blades arranged to simulate those in a turbomachine. The

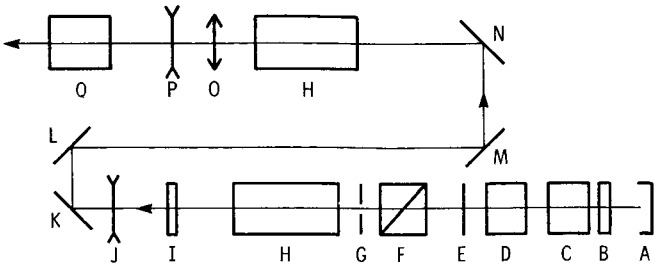

A	Concave mirror, 5-m radius of curvature	H	Flashlamps and Nd-YAG rods
B	Etalon	I	Plane output coupler
C, D	Pockels cells	J	Diverging lens
E	Quarter wave plate	K, L M, N	45^0 Turning mirrors
F	Glan Taylor prism	O, P	Reducing telescope
G	1.5-mm Pinhole	O	Frequency doubling crystal

Figure 1.—Schematic of double-pullse, Q-switched, frequency-doubled Nd:YAG laser with stable or TEM_{00}oscillator.

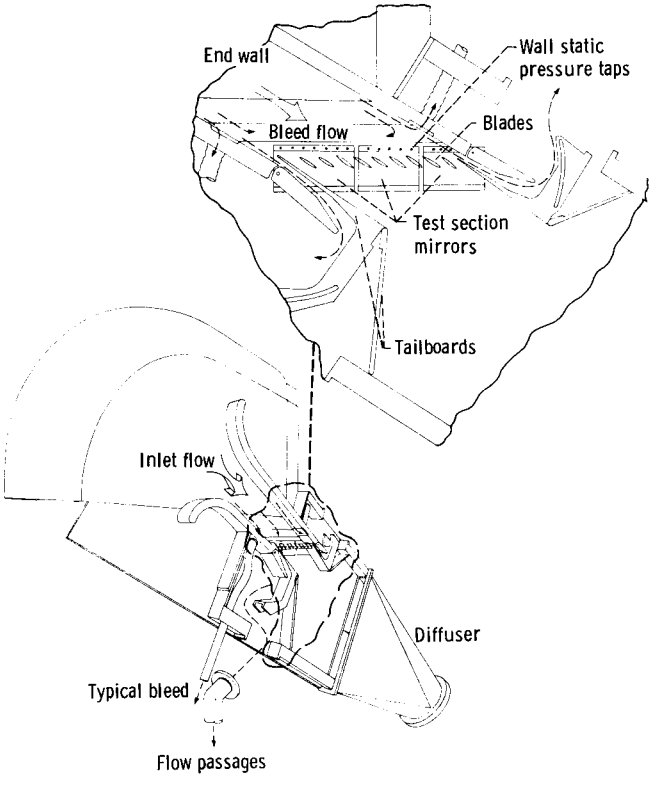

Figure 2.—Schematic of flutter cascade.

blades, in addition, can be driven externally to vibrate about a midchord axis to simulate the forcing functions expected in aeroelastic instability or flutter (refs. 11 and 12). These blades, vibrating in a pitching motion about the midchord axis, in turn, create time-varying flow conditions for the three-dimensional imaging of flow features by diffuse-illumination, double-exposure holographic interferometry. The flutter cascade also affords an excellent view of the flow passages between the blades, making it easy to adjust the view for best visualization of a flow feature. In particular, one can adjust the view to

be arbitrarily close to the tangency to a shock-wave surface for best three-dimensional visualization of the shock wave. A typical arrangement of the holographic setup and blades is shown in figures 3 and 4. A 70-mm motion picture camera, with lenses removed (foreground of fig. 4) was used as a film transport. Holograms were recorded on this film as the blades were vibrated.

The laser system produced positive results (refs. 13 and 14). Figure 5 shows photographs of several reconstructed images from several holograms, or frames, of the time-varying shock-wave structure in a three-blade flutter cascade. In the actual reconstructed images the shock-wave structure appears as hair-like or as filaments hanging from the blades.

The advantages of this laser configuration were the narrow line width (less than 0.01 cm^{-1}), the consequential good coherence (coherence length more than 1 m), and the relatively smooth Gaussian beam profile. These features were available at 20 double exposures per second, with exposure separations adjustable from 1 to 100 μsec. The major weakness was the low energy of 10 mJ of 532-nm light per double exposure. In the flutter cascade the object beam is derived by passing

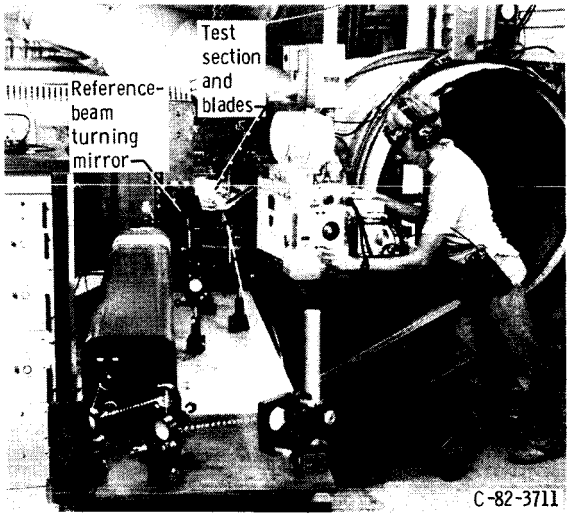

Figure 3.—Setup for holographic cinematography in three-blade flutter cascade.

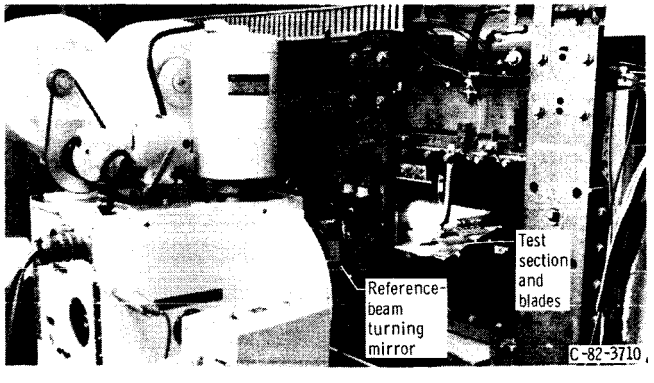

Figure 4.—View of blades and film transport for recording holographic motion pictures in three-blade flutter cascade.

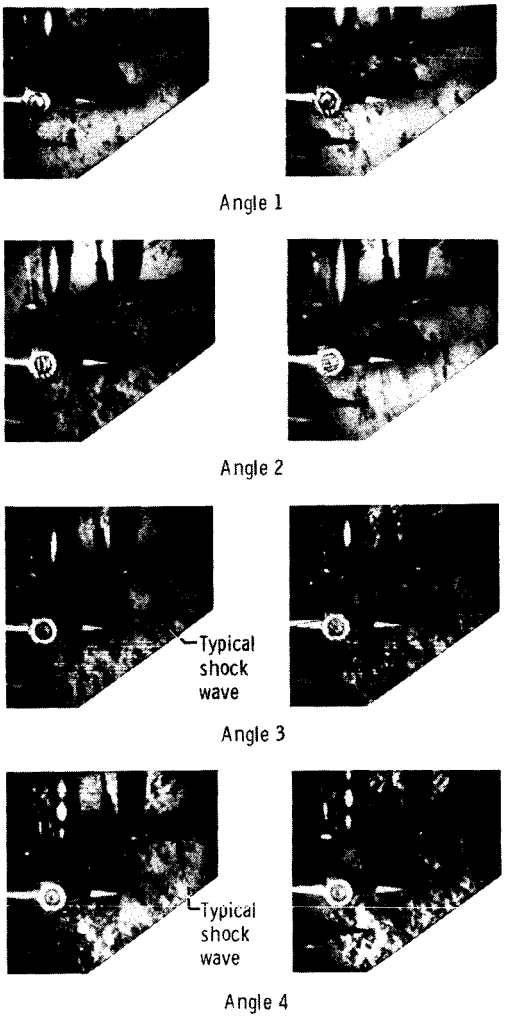

Figure 5.—Reconstructed images from holograms of shock structure in three-blade flutter cascade.

the object illumination through a window to the tunnel back wall, by diffusely reflecting this light from the back wall, and by recording the beam after it has passed back out through the window. For this application, the 10-mJ per double exposure proved to be marginal.

Simple attempts to increase the energy of the laser proved fruitless: An increase in the diameter of the transverse aperture in the oscillator produced higher order modes, and a double-pass amplifier produced instability due to feedback. Rather than adding a second amplifier stage, the laser oscillator was reconfigured to yield more energy.

Second Configuration of the Laser System

The second configuration of the laser system included a transmission coupled unstable resonator and a single-pass amplifier (fig. 6). Most commercially available Q-switched Nd:YAG lasers use unstable resonators, where a light ray passing back and forth between the reflectors in the laser oscillator does not retrace its path. In the stable resonator the light ray retraces its path. (The properties of unstable

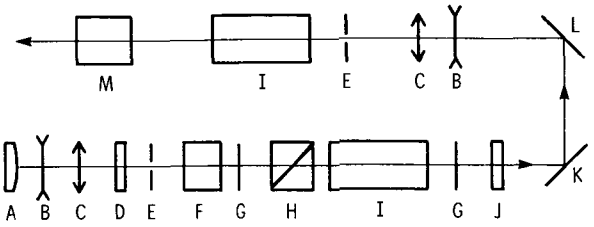

A	Convex mirror, 3-m radius of curvature	G	Quarter wave plate
B, C	Telescope	H	Glan Taylor prism
D	Etalon	I	Flashlamps and Nd-YAG rods
E	Spatial filter	J	Plane output coupler
F	Pockels cells	K, L	45^0 Turning mirrors
		M	Frequency doubling crystal

Figure 6.—Schematic of double-pulse, frequency-doubled Nd:YAG laser with transmission coupled unstable oscillator.

resonators are described in the literature (ref. 15).) Most commercially available unstable resonators used in Nd:YAG laser systems employ polarization or diffraction coupling to couple energy out of the oscillator cavity. The holographic laser of figure 6 uses transmission coupling through the plane reflector. This configuration was chosen to yield a narrower line width in both exposures of the double exposure, using relatively simple optical parts. In fact, most of the optical components in the laser were identical with those of the former configuration. However, a new Q-switch was used to increase the energy stability from pulse pair to pulse pair and the shot-to-shot stability of the energy ratio between pulses of a pulse pair (to within 10 percent).

The new configuration showed an energy increase up from 10 to 100 mJ per double exposure at 532 nm. The line width, however, increased to slightly less than 0.03 cm^{-1}. Hence, the coherence length was only about 30 cm. The beam uniformity was less than that of the previous laser system. The hologram recording rate was still 20 double exposure holograms per second.

The new laser configuration was evaluated in a larger flutter cascade than the one used to evaluate the first. The larger flutter cascade (fig. 2) has nine blades, which vibrate over an angle-of-attack range of $\pm 1.2°$ about a mean angle of attack of 7° (ref. 16). Upstream Mach numbers are generally set at 0.80 or 0.85, and the vibrational frequencies are either 200 or 500 Hz. The interblade phase angle is adjustable; that is, the blade drive mechanism can be adjusted so that adjacent blades achieve their maximum angles of attack at different times in the vibrational cycle. The typical values chosen are $\pm 90°$ and 0. For $+90°$ a blade achieves its maximum angle of attack while adjacent blades are at the mean angle of attack. At 0 all blades vibrate in phase.

The holographic setup used to evaluate the laser was essentially the same as that used in the other cascade (fig. 7). Again, the object beam was derived by reflection from the diffuse surface of the back sidewall of the tunnel. The reference beam was reflected back to the holographic emulsion (contained on the 70-mm film) from a mirror attached to the tunnel. This reference-beam configuration provides some compensation for rigid motions of the tunnel.

The laser, which can be triggered stroboscopically, can be synchronized, in principle, to record holograms at discrete, but monotonically changing, angles of attack. A time history of a shock wave (whose geometry is a function of the angle of attack) can be determined in this manner. The 20-Hz capability of the laser permits expeditious recording of the time history.

Comparison of the Two Laser Configurations

From the viewpoint of holographic flow visualization, the interesting result is that the two laser configurations yielded the same quality flow visualization. The photographs of reconstructed images of several flow conditions in the larger flutter cascade recorded with the unstable (second configuration) resonator (fig. 8) can be compared with the results obtained with the stable (first configuration) resonator (fig. 5).

Note that the two laser configurations produce beams with different properties of coherence, uniformity, and energy and that they were evaluated in different flutter cascades. The application involving the stable resonator (figs. 3 to 5) required pulse separations of 5- to 15-μsec; the application involving the unstable resonator (figs. 7 and 8) required pulse separations of 15- to 30-μsec. Still, the results are quite similar.

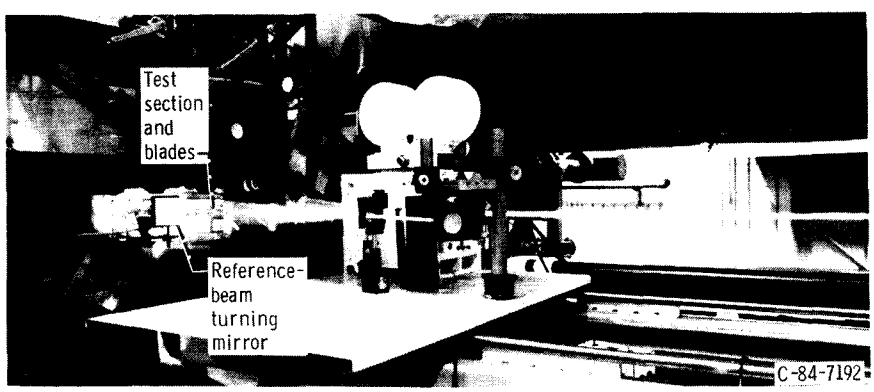

Figure 7.—Setup of holographic cinematography in a nine-blade flutter cascade (four blades in field of view).

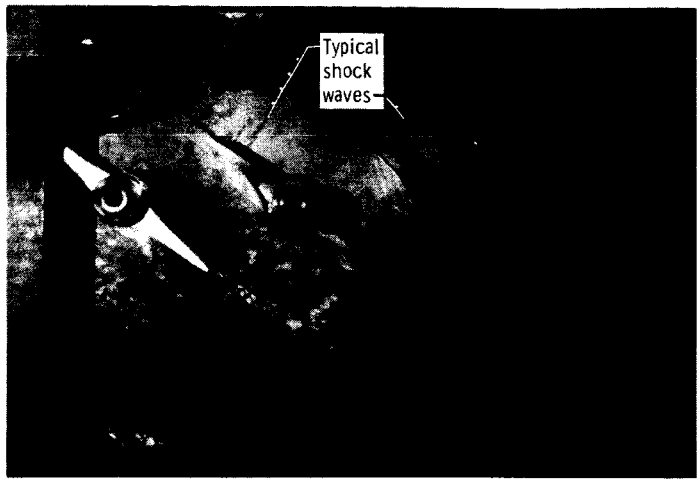

Figure 8.—Reconstructed images from holograms of shock structure in nine-blade flutter cascade.

The holographic images are substandard. Since the laser design did not affect the quality of the holographic images, another explanation must be found for their inferior quality. In an attempt to find an explanation,the next main section evaluates the holographic process itself.

Holography

The holographic process is now thoroughly (and at times usefully) described in books (refs. 17 to 21). The discussion in this paper begins with a brief review of holography, followed by a presentation of the complications and defects of the actual holographic process. An attempt is made to support the conclusions concerning the defects of the holographic process in the flutter cascades.

Review

The simplest possible representation of a hologram is as a linear, two-dimensional recording of the interference between two complex, monochromatic, scalar, light waves, $O(r)$ and $R(r)$. In such a recording $O(r)$ contains information about an object (e.g., the change of phase of light that has passed through a flow field) and is called the object wave. The wave $R(r)$ is chosen to have a simple form (e.g., plane or spherical) so that it can be duplicated easily at a later time and is called the reference wave. The position, a vector, is represented by the scalar r for simplicity. The objective of holography is to record the phase of $O(r)$ relative to $R(r)$.

The simple representation of a hologram is then given by

$$T(r_h) = B(|O|^2 + |R|^2 + OR^* + O^*R) \qquad (1)$$

where T is the transmittance of the processed recording to the field (as opposed to the intensity) of an incident scalar wave, B is a proportionality constant, r_h is a position on the hologram, and * denotes the complex conjugate.

If the simplest of holograms is illuminated by an exact duplicate of the reference wave $R(r)$ (now called the reconstruction wave), the output is the scalar wave:

$$RT = BR(|O|^2 + |R|^2) + B|R|^2O + BRRO^* \qquad (2)$$

The output consists of three independent waves, (1) $BR(|O|^2 + |R|^2)$, (2) $B|R|^2O$, and (3) $BRRO^*$. The most significant, from the viewpoint of three-dimensional flow visualization, is the second. That wave is proportional to the original object wave at the hologram aperture. If $B|R|^2 = 1$, then the second wave is an exact duplicate of the object wave. The second wave is sometimes called the reconstructed object wave. It can be propagated analytically either forward or backward in time using a diffraction integral or the methods of geometrical optics. If propagated backward in time, the wave is imagined to enter a virtual-image space in front of the hologram. If propagated forward in time, it is imagined to enter a real-image space. Most three-dimensional images viewed in holography appear to come from the virtual-image space. The hologram itself can be treated like any other aperture in an optical imaging system.

The only defect in this ideal process is its low efficiency for diffracting the reconstruction wave into the reconstructed object wave. To understand the source of this low efficiency, note that the three reconstructed waves are separated spatially at a sufficient distance from a standard off-axis-reference-beam hologram. (In an off-axis-reference-beam hologram the optical axes of the object and reference beams are separated by a fairly large angle.) When the three beams are separated spatially, their intensities can be considered independently. (If the beams overlap, they interfere.) The maximum efficiency occurs when $|R|^2 = |O|^2$.

For this case, the intensities in the three waves, respectively, are given by $4B^2|R|^6$, $B^2|R|^6$, and $B^2|R|^6$. The efficiency is then given by

$$\frac{B^2|R|^6}{6B^2|R|^6} = 17 \text{ percent}$$

In fact, the maximum efficiency of a two-dimensional hologram in a silver halide emulsion does not exceed 4 to 6 percent. The reason is that $|R|^2$ is chosen to be many times $|O|^2$ in order to avoid nonlinear noise in the reconstructed image.

The Holographic Process and its Defects

The actual holographic process can deviate considerably from the ideal. Fortunately, at its worst, holography usually does a creditable job of replicating the phase of a light wave. The factor $B|R|^2$ in the reconstructed wave can be a function of position, but, as long as it is real, the reconstructed wave contains the exact phase of the object wave.

The two effects of deviations of the holographic process from the ideal are

(1) A reduction (or an increase) in the brightness of the reconstructed image

(2) An introduction of several sources of noise.

The terms frequently used to refer to a holographic image suffering from these defects are "nonexistent, muddy, dirty, washed out, low contrast, hazy, fuzzy, faint, narrow field, and shallow."

Some of these same terms can apply to certain applications of double-exposure, diffuse-illumination interferometry as a three-dimensional imaging technique, even if the holographic process is flawless. This section is restricted to single-exposure holograms. Some readers may find it useful to read the review of interferometry in the next main section, since holography is an application of interferometry.

Deviations from the ideal holographic process that require definition and analysis are

(1) Nonlinear recording and other complications in using silver halide emulsions

(2) Nonmonchromaticity of the laser

(3) Polarization effects

(4) Random phase of the object wave when using a diffuser

(5) Modulation of the object and reference waves due to rig vibration and motion

(6) Phase holograms and bleaching

(7) Extraneous waves and specular reflections.

First, the complications of using silver halide emulsions are discussed and related to the holograms reported herein.

Silver halide emulsions—Silver halide emulsions specifically intended for holography are manufactured in the United States, Belgium, Japan, and the Soviet Union. The most recent and extensive published work on silver halide emulsions for holography originates in the Soviet Union (ref. 22). The book by Collier, Burckhardt, and Lin (ref. 17) is still an excellent reference on the use of silver halide emulsions for holography. The analytical approach of that book is used in this paper. Summaries of the properties of silver halide emulsions can be found in reference 18 (edited by Caulfield). Manufacturers' literature is also a source of properties. The holographic properties of some emulsions have been reported in papers; for example, see Landry and Phipp's results for the Agfa-Gevaert Scientia 10E75 emulsion (ref. 23).

The holograms discussed herein were recorded on the Kodak SO 253 panchromatic emulsion on 70-mm Estar film, prepared for use in the Mitchell DA 70 camera, and on the Afga-Gevaert 10E56 orthochromatic emulsion on 4- by 5-in. glass plates. (It is more informative to list emulsion and development-procedure combinations.) Most of the holography literature in the United States discussed development using Kodak D-19 developer, a high-contrast, solution-physical developer.

For this report individual holograms and short strips of 70-mm film were hand developed using Kodak D-19. Longer rolls of 70-mm film were developed in an automatic film processor, using another active developer, Kodak Duraflo Rt A and B. There were no obvious developer-caused differences in the reconstructed images.

The holograms were also converted to phase holograms by bleaching, a technique whose performance is discussed in more detail later. The bleach was potassium ferricyanide plus potassium bromide. This particular bleach worked by refractive index modulation rather than thickness modulation.

The total procedure (exposure, development, and bleaching) has about the same technical rigidity as the selection and application of house paint. It is best summarized by stating that the results obtained at NASA Lewis have at least been consistent over several years. Seldom has a processing failure been a cause of poor hologram quality, although processing defects such as emulsion shrinkage have been significant at times.

Characterization of the holographic performance of silver halide emulsions.—Equation (1), for an ideal silver halide emulsion, assumes the modified form

$$T = A - B'(E_0 + t_e OR^* + t_e O^* R) \tag{3}$$

where A is a constant, B' is a constant, t_e is the exposure time, and E_0 is the average exposure, given by

$$E_0 = t_e(|O|^2 + |R|^2) \tag{4}$$

As in common practice, a specific set of units and dimensions is not indicated. On reconstruction with an exact duplicate of the reference wave R, the reconstructed object wave is given by the scalar field $-B' t_e |R|^2 O$ and the intensity of this wave is given by $|B'|^2 t_e^2 |R|^4 |O|^2$.

The efficiency of the reconstruction process is obtained by dividing the intensity of the reconstructed object wave above by the intensity $|R|^2$ of the reconstruction wave, with the result given by

$$\eta = |B'|^2 t_e^2 |R|^2 |O|^2 \tag{5}$$

In the absence of certain complicating effects (to be discussed later), the modulation of the intensity used to record a hologram is often expressed by the interference-fringe visibility, the fringe visibility, or simply the visibility. It is exactly true for plane waves and roughly true for the waves used to record a hologram that the local exposure varies over the range $(E_0 \pm 2t_e|O||R|)$. The visibility V is given by

$$V = \frac{2t_e|O||R|}{E_0} \tag{6}$$

and is the difference locally between the maximum and minimum exposures divided by the sum of the maximum and minimum exposures. In terms of visibility, equation (5) becomes

$$\eta = \frac{|B'|^2}{4} V^2 E_0^2 \tag{7}$$

As used by reference 17, the square root of equation (7) is the more useful expression, where

$$\sqrt{\eta} = |S| V E_0 \tag{8}$$

and

$$|S| = \frac{|B'|}{2}$$

Hence, for a perfectly linear recording in a silver halide emulsion (or in any recording material), the square root of the diffraction efficiency, η is proportional to the visuality V and to the average exposure E_0.

Self-interference and nonlinear noise.—In a real silver halide emulsion, $\sqrt{\eta}$ is linear only over a limited range of exposures E_0 and visibilities V. Also, in general, S is a complex function of both exposure and visibility.

For real silver halide emulsions, there is an exposure E_0 that maximizes the linear range of $\sqrt{\eta}$ versus V and an exposure that maximizes η. Fortunately, the maximum linear range yields efficiencies that are close (but not equal) to the maximum values available (about 4.5 percent). Reconstructing an image of high quality requires that the nonlinear portion of equation (8) be avoided.

The typical exposure for an optimum linear recording of a two-dimensional, amplitude-modulation hologram (the kind expressed by eqs. (1) and (3)) is an exposure that produces a photographic density around 0.8. Ordinary black and white photography is accomplished with photographic densities that vary generally from 0.6 to 2.5.

When recorded correctly, the amplitude-modulation hologram yields beautiful images. The holographic motion pictures reported in reference 10 were composed of this type of hologram. But amplitude-modulation holograms are not suitable for wind-tunnel applications. They suffer from the following defects:

(1) The optimum exposure is quite critical for an amplitude modulation hologram and can vary from one sample of an emulsion type to another. A scan of manufacturers' literature, suppliers' literature, and the references shows recommended exposures for the Agfa-Gevaert 10E56 emulsion at 532 nm to range from 1.0 to 3.0 $\mu J/cm^2$ and for the Kodak SO 253 emulsion to range from 2.0 to 4.0 $\mu J/cm^2$. The actual optimum exposure also depends on the development time, condition of the developer, and the temperature of the developer. These variables might mean the difference between no image and an excellent image.

(2) The effective sensitivity of the emulsion is reputed to decrease with the time elapsed between the exposure and the processing of the hologram. It is recommended that processing be accomplished within 30 min of recording (ref. 18). In practice, several hours may elapse in the case of a glass-plate hologram, and several days may elapse in the case of a roll of film.

For a heavy enough exposure, the exposure of a bleached hologram is not critical. The hologram can be heavily exposed (see the discussion of bleached holograms below) so that a decrease in sensitivity with time is not destructive. The bleached hologram is also more efficient, but holograms are bleached mainly for consistency of performance.

Fortunately, equation (8) can be used to characterize any recording material and process, including both bleached and unbleached holograms. The discussion of noise is the same. The objective always is to operate within the dynamically linear portion of the emulsion characteristic. Otherwise, the signal-to-noise ratio (ratio of intensity in the image to all other detected intensities) is degraded. The major source of noise for a bright image is from the self-interference terms $B(|O|^2 + |R|^2)$ of the hologram.

In a perfectly linear recording, such as expressed by equations (1) and (3), this source of noise is avoided by satisfying the off-axis-reference-wave criterion (ref. 17). That criterion states that, if the half-angle of the object field of view is θ_o, then the angle θ_r between the object and reference wave axes must satisfy

$$\sin \theta_r > 3 \sin \theta_o \tag{9}$$

For example, if the full angle of the object field is 20°, then the off-axis-reference-wave criterion is that $\theta_r > 31.4°$. This criterion follows from the fact that the $B|O|^2$ term of the hologram (eq. (1)) diffracts light into about twice the full angle of the object wave itself. Hence, about three object-wave half angles of beam-axis separation will prevent extreme rays of the object and self-interference waves from overlapping. This criterion should be satisfied for all light waves recorded by the hologram—including any noise waves, such as specular reflections from blades or windows.

Once the self-interference noise has been avoided by satisfying the off-axis-reference-wave criterion, the objective is to avoid reintroducing that noise by nonlinear effects. The major nonlinear effect is of second order in the exposure. To include this effect, equation (1) must be expanded to second order to become

$$T = B(|O|^2 + |R|^2 + OR^* + O^*R) + C(|O|^2 + |R|^2 + OR^* + O^*R)^2 \qquad (10)$$

The term that varies as the square of the original intensity contributes a reconstructed wave $2C|O|^2|R|^2O$; consequently, the self-interference noise is reimposed about the axis of the reconstructed object wave.

The nonlinear region of equation (8), and, consequently, the reimposition of self-interference noise, are avoided by choosing a beam ratio ($P = |R|^2/|O|^2$) that is much greater than unity. In the absence of reduced coherence and depolarization (to be discussed later), the visibility is given by

$$V = \frac{2\sqrt{P}}{1 + P} \qquad (11)$$

Plots of equation (8) reveal that (ref. 17) the maximum visibility V that can be rationalized to yield linear recording is 0.8 The corresponding beam ratio P, determined from equation (11), is 4.

Although beam ratios as low as 4 to 1 are used in holography, this average beam ratio does not account for local fluctuations in the object-wave intensity. The worst local fluctuation is due to the laser speckle effect. The local intensity I (as opposed to the average intensity $<I>$) of the object wave, when speckle effect is important, is defined by the probability density (ref. 27)

$$p(I) = \frac{\exp(-I/<I>)}{<I>} \qquad (12)$$

Speckle fluctuations are substantial, since the standard deviation of this distribution equals the average intensity $<I>$ itself. Hence, there is a significant probability of a local intensity of $2<I>$ or even $3<I>$. If these fluctuations are to avoid entering the nonlinear region of the emulsion characteristic, the average beam ratio must be increased to between 8 and 12.

When nonlinear noise is the major source of noise, signal-to-noise ratios around 100 are achieved with visibilities around 0.4. For two standard deviations of the laser speckle effect to produce fringes with a visibility V no larger than 0.4, the required average beam ratio P must be no smaller than 69. However, for reconstructed images as faint as implied here, other sources of noise such as scattering are important.

In fact, because of depolarization, the holograms reported herein were recorded with an effective beam intensity ratio P of about 10. This ratio is large enough to cover one standard deviation of the laser speckle effect, according to the analysis above. However, the major source of noise experienced was not nonlinear noise, at least not from the endwall diffuser, which is the source of the laser speckle effect. The visibility V can be affected by factors other than the beam ratio. In any case, it was observed that increasing the beam ratio had no obvious effect on the quality of the reconstructed images.

Comparison of SO 253 and 10E56 emulsions.—With the holographic setups used in the flutter cascades, the 10E56 emulsions produced a somewhat brighter reconstructed image than did the SO 253 emulsion. The observed difference in performance between the two emulsions probably can be attributed to a difference in emulsion thickness.

The emulsions have similar sensitivities and resolutions at 532 nm, and their exposure ranges overlap. The published resolutions of the emulsions are about 2500 cycles/mm.

The two emulsions have different thicknesses. The SO 253 emulsion is 9 μm thick, and the 10E56 emulsion is 6 μm thick. The thickness of an emulsion is primarily important in establishing a Bragg diffraction criterion wherein the hologram is no longer considered to be two-dimensional. Each pair of spatial frequency components of the object and reference waves (the plane-wave components obtained by performing Fourier transformations of the mathematical expressions for the object and reference waves) interfere. The interference maxima are planes that extend through the thickness of the emulsion. For maximum brightness in reconstruction, the angle of each component of the original reference wave must be duplicated. Unfortunately, this duplication is more easily said than done. Typically, the wavelength of the beam used to record the hologram is different from that used to reconstruct the image. For example, the wavelength of the second harmonic of the Nd:YAG laser is 532 nm. The hologram recorded using that laser might be reconstructed using an argon-ion laser at 514.5 nm or even a helium neon laser at 633 nm. The other complication is shrinkage of the emulsion during processing. Shrinkage introduces a spatial-frequency-dependent variation in the change between the separations of interference planes. These effects can be minimized and compensated for only in part.

These thickness effects are less important for the thinner 10E56 emulsion than for the SO 253 emulsion. The angular deviations that can be tolerated in the components of the reconstruction wave are inversely proportional to the emulsion thickness. A somewhat brighter image is probably to be expected from the 10E56 emulsion.

One possible conclusion is that a thinner emulsion should be selected when beam arrangements or hologram processing are not the optimum. However, the main consideration in selecting an emulsion is its availability on the commercial market at the time of purchase.

Other factors may also affect the quality of holograms. The choice of beam ratio, for example, may be determined in part by the temporal coherence of the laser, a topic discussed below.

Coherence and beam polarization effects.—Visibility V (as defined by eq. (6)) does not necessarily depend only on the beam ratio P as implied by equation (11). When coherence and polarization effects are important, the visibility is better expressed by

$$V = \frac{2\,|\mu(\Delta l)|\sqrt{\psi}\,\sqrt{P}}{1+P} \tag{13}$$

where $|\mu(\Delta l)|$ is the magnitude of the complex degree of temporal coherence (for a spatially coherent laser), Δl is the optical path length difference between an interfering reference-ray–object-ray pair, and ψ is a depolarization coefficient.

The complex degree of temporal coherence $\mu(\Delta l)$ can be calculated from the detailed spectrum of a quasimonochromatic laser beam (a laser beam for which dispersion on propagation is negligible). But there is a performance oriented estimate of coherence available in holography. To make that estimate, a low-beam-ratio hologram (4 or even 3 to 1) is recorded of an inclined plane, and the depth of the brightly reconstructed portion is measured. The objective is to let $|\mu|$ alone determine the depth of the object field (extent of Δl) that can be observed. The pattern observed on the inclined plane also contains some information about the functional form of $|\mu(\Delta l)|$ and the spectrum of the laser. For example, a beam consisting of nearby laser modes with constant relative phases can produce a rather complicated pattern of fringes.

When the estimate of coherence was performed on the Nd:YAG lasers tested at Lewis, the brightly reconstructed region was smooth, and there was little visible outside that region. The scene depth D of the bright image approximately satisfied the relationship

$$D = \frac{1}{2}\Delta l_{\max} = \frac{1}{2\Delta(1/\lambda)} \tag{14}$$

Here, $\Delta(1/\lambda)$ is a frequently quoted specification, the full width of the laser spectrum at half-maximum power. For example, if the spectral width is 0.03 cm^{-1}, then the depth of the scene that can be recorded brightly is about 15 cm. The scene depth can be used to estimate the width of a diffuser that can be recorded brightly. For example, if a hologram is recorded of a diffuser at a distance of 50 cm, then path variation of 15 cm on either side of the diffuser center corresponds to a diffuser width of 83 cm. The flutter-cascade fields of view did not approach this size.

A reduction in coherence $|\mu|$ decreases the visibility V and the hologram efficiency η. These decreases can be compensated for by decreasing the beam ratio P, without increasing the V-dependent nonlinear noise, but the practicality of this adjustment is limited: a factor of two decrease in P requires approximately twice the laser pulse energy.

Path matching (refs. 2 and 3) can be used to maintain a constant value of $|\mu|$ over the observed field. This fix may be necessary, when using a very incoherent laser, or when rapid variations in $|\mu|$ will produce a confusing pattern.

The other coefficient ψ accounts for differences in polarization between the reference and object waves. In equation (1) the object-wave term BOR^* should actually be replaced by a vector expression $B\mathbf{E}_o \cdot \mathbf{E}_r$ where the vectors represent the spatial parts of the electric fields of the object and reference waves. Then, $\sqrt{\psi}$ is the cosine of the angle between these two vectors. The coefficient ψ represents the reduction in efficiency of the hologram due to relative depolarization of the two vectors.

Depolarization is caused by using a depolarizing diffuser, by reflections, by birefringance in the laser amplifer(s), or by wave-front curvature. Depolarization may be required when low-quality optical windows are used (ref. 24). Also, depolarization is a necessary feature of one system that minimizes the recording of specularly reflected object waves (as covered later).

Note also that equation (13) is written with well-defined values of $|\mu|$ and ψ. Yet the performance-oriented test of coherence uses an object (e.g., an inclined plane) where the coherence and the depolarization may vary over the entire object. The object is diffusely reflecting, so that each point on the hologram receives light from all points on the object. Single values of $|\mu|$ and ψ do not apply in this case. The treatment of an object wave from a diffusely reflecting object (e.g., the back sidewall of the flutter cascade) is discussed briefly next.

Diffuse object waves.—There is a linear theory of the propagation of light, applied here from a diffuser point $\mathbf{r}_d$ to a hologram point $\mathbf{r}_h$ (ref. 25). The object wave at the hologram is given by

$$O(\mathbf{r}_h) = \int h(\mathbf{r}_h,\mathbf{r}_d)O(\mathbf{r}_d)\,d\mathbf{r}_d \tag{15}$$

where the function $h(\mathbf{r}_h,\mathbf{r}_d)$ of the diffuser and hologram positions is called the impulse-response function of the recording system. This function can include the effects of propagation, lenses, apertures, spatial filters, and other linear beam-modification processes. In fact, the entire holographic process, from recording to final reimaging of the reconstructed image by the eye, can be represented approximately by a single impulse-response function. Before doing this, consider the hologram itself.

Equation (1) for the hologram can easily be modified to include the linear theory, and to include equation (13) as well. The result is given by

$$T(\mathbf{r}_h) = B\Big(|O(\mathbf{r}_h)|^2 + |R(\mathbf{r}_h)|^2 + R^*(\mathbf{r}_h)\int h(\mathbf{r}_h,\mathbf{r}_d)|\mu(\mathbf{r}_h,\mathbf{r}_d)|\sqrt{\psi(\mathbf{r}_h,\mathbf{r}_d)}\, O(\mathbf{r}_d)\, d\mathbf{r}_d + R(\mathbf{r}_h)\int h^*(\mathbf{r}_h,\mathbf{r}_d)|\mu(\mathbf{r}_h,\mathbf{r}_d)|\sqrt{\psi(\mathbf{r}_h,\mathbf{r}_d)}\, O^*(\mathbf{r}_d)\, d\mathbf{r}_d\Big) \tag{16}$$

where the object dependent variations of ψ and $|\mu|$ are specifically indicated. It can be seen from equation (16) that the linear theory assures that each product $|\mu|\sqrt{\psi}O(\mathbf{r}_d)$, and, therefore, each object point records a hologram independently of the other object points. The overall hologram is a sum (integral) of these independent holograms.

The linear theory is also easily incorporated in equation (5) for the efficiency, where

$$|O|^2 = \iint h(\mathbf{r}_h,\mathbf{r}_d)h^*(\mathbf{r}_h,\mathbf{r}_d')|\mu(\mathbf{r}_h,\mathbf{r}_d)|\,|\mu(\mathbf{r}_h,\mathbf{r}_d')| \sqrt{\psi(\mathbf{r}_h,\mathbf{r}_d)\psi(\mathbf{r}_h,\mathbf{r}_d')}\, O(\mathbf{r}_d)O^*(\mathbf{r}_d')\, d\mathbf{r}_d\, d\mathbf{r}_d' \tag{17}$$

As pointed out in the use of equation (12), the object wave from the diffuser is a random variable. Furthermore, it is common practice to take the phases of $O(\mathbf{r}_d)$ and $O^*(\mathbf{r}_d')$ as independent random variables. Then, the expectation value of $|O|^2$ is used in equation (5) to calculate an average efficiency. The expectation value is given by

$$\langle|O(\mathbf{r}_h)|^2\rangle = g\int|h(\mathbf{r}_h,\mathbf{r}_d)|^2|\mu(\mathbf{r}_h,\mathbf{r}_d)|^2 \psi(\mathbf{r}_h,\mathbf{r}_d)|O(\mathbf{r}_d)|^2\, d\mathbf{r}_d \tag{18}$$

where g is a proportionality constant. Hence, each diffuser point contributes its own efficiency independently. That efficiency $d\eta$ is the integrand of equation (18) multiplied by $|B'|^2t_e^2|R|^2$ as in equation (5).

The performance-oriented test of coherence involves viewing the reconstructed three-dimensional image of a diffusely reflecting inclined plane, rather than the hologram itself. As state before, this is best handled with a single impulse-response function covering the entire holographic process. The effects of coherence and depolarization are easily represented, provided that both are approximately independent of the hologram coordinates. This assumption is reasonable, since the hologram, or part of the hologram, used in imaging is usually small. Then the reconstructed image, reimaged by the eye, or a camera, has an expected intensity of

$$\langle|O(\mathbf{r}_i)|^2\rangle = g'\int|h(\mathbf{r}_i,\mathbf{r}_d)|^2|\mu(\mathbf{r}_d)|^2 \psi(\mathbf{r}_d)|O(\mathbf{r}_d)|^2\, d\mathbf{r}_d \tag{19}$$

where g' is another proportionality constant and the subscript i refers to the final image.

Of course, the impulse-response function is different from the one indicated in equation (18). The impulse-response function is now quite narrow. Not including a possible magnification factor in imaging results in a $h(\mathbf{r}_i,\mathbf{r}_d)$ value of nearly zero, unless $\mathbf{r}_i = \mathbf{r}_d$. For $\psi = 1$ the observed intensity at $\mathbf{r}_i = \mathbf{r}_d$ is proportional to the object intensity multiplied by $|\mu(\mathbf{r}_d)|^2$, and the performance-oriented test of coherence is exactly correct. More generally, the test, which is an evaluation of $\psi|\mu|^2$, is affected by variations in the intensity of the object illumination, and assumes that the intensity is averaged over many speckles, where the speckle effect represents the second-order statistics of the fluctuating object field. The process of viewing a reconstructed image averages over the high-frequency fluctuations of that field; that is, many speckles are averaged. However, the hologram itself records these high-frequency fluctuations, and, as discussed above, care must be exercised to avoid nonlinearities. The exact nature of the field at the diffuser is unimportant for the analysis involving nonlinearities. Note also that the analysis regarding beam ratios and speckle statistics was presented for a perfectly coherent, polarized object wave. The average product of coherence and polarization may be less than unity, making a smaller beam ratio tolerable.

If the diffuser should move substantially during an exposure, the holographic results can be affected adversely. The next section treats the effects of object motion during the exposure.

Rig vibration and motion.—In principle, there are two reasons that rig vibration and motion affect a hologram adversely: decorrelation and definite-phase variations. The effect is similar to a reduction in coherence and can be regarded as a reduction in coherence, since the spectrum of the object wave is changed.

Motion during an exposure is handled by substituting the time average of the object wave in the expressions for a hologram (eqs. (1), (3), (10), and (16)). The time-averaged object wave is given by

$$\bar{O}(\mathbf{r}_h) = \frac{1}{t_e}\int_0^{t_e} O(\mathbf{r}_d,t)\, dt \tag{20}$$

where $O(\mathbf{r}_h,t)$ contains time variations at other than the optical frequency. From the object wave at the object itself, the object wave at the hologram is given by

$$\bar{O}(r_h) = \frac{1}{t_e}\int_0^{t_e}\int h(\mathbf{r}_h,\mathbf{r}_d,t)O(\mathbf{r}_d,t)\, dr_d\, dt \tag{21}$$

where the linear theory is specifically applied. Note that motion of the recording components is included in a possible time variation of the impulse response function.

From a diffuser the phase of O has a deterministic component and a random component. A variation in the random part of the phase is called decorrelation. Decorrelation

is caused mainly by motion of the diffuser perpendicular to a light ray and, possibly, by turbulence. Definite-phase variations are caused mainly by motion along a light ray.

Significant decorrelation requires a transverse motion equal to the resolution of the overall recording system. This resolution is likely to be several wavelengths of light. Significant, definite-phase variations are caused by path changes of a fraction of the wavelength of light. Hence, definite phase variations are most likely to degrade a hologram first. An exception would be a high-speed, transverse moving object, such as a rotating component.

If an object is moving so that the definite object-ray–reference-ray path difference is changing at a rate v, then the reconstructed brightness of an object point will be proportional to the factor (ref. 14)

$$|\mu_v|^2 = \left[\frac{\sin(\pi v t_e/\lambda)}{\pi v t_e/\lambda}\right]^2 \tag{22}$$

This factor equals its first zero at $v = \lambda/t_e$. When $t_e = 15$ nsec, a typical exposure for a holographic Nd:YAG laser, then $v = 36$ m/sec for a zero.

For a negligible effect, it is required that $|\mu_v|^2 < 0.9$ and $v < 6$ m/sec. To reach 6 m/sec, the vibrational levels would have to be orders of magnitude larger than measured.

It is very unlikely (but not totally out of the question) that object motion would degrade a single-exposure hologram. As discussed later, decorrelation and definite phase variations both can be significant in double-exposure holography.

Phase holograms—bleaching.—The results presented so far will be modified only slightly for bleached holograms. An ideal phase hologram retards the phase of an incident wave in proportion to the original exposure; that is, the ideal holograms of equations (1) and (3) are converted to ideal phase holograms when their amplitude transmittances are given by

$$T'(\mathbf{r_h}) = \exp[jFT(\mathbf{r_h})] \tag{23}$$

where $T(\mathbf{r_h})$ represents the original linear hologram and F is a constant.

The process for converting a silver halide hologram to a phase hologram is called bleaching. Bleaching was mentioned briefly in the discussion of silver halide emulsions. It was also mentioned that the linearity relationship (eq. (8)) is used also to characterize phase holograms.

The fact that both phase and amplitude-modulation holograms are characterized by the same linearity relationship can be explained using a little algebra. First, the object wave O and the reference wave R are expressed specifically in terms of their magnitudes and phases:

$$O = U_o \exp j\varphi_o \qquad R = U_r \exp j\varphi_r$$

When these expressions are substituted in equation (3) for an ideal silver halide hologram, that expression becomes

$$T = A - B'E_0 - 2B't_eU_oU_r \cos(\varphi_o - \varphi_r) \tag{24}$$

Ideal bleaching converts equations (24) (via eq. (23)) into the ideal phase hologram

$$T'(r_h) = A' \exp[j\beta t_eU_oU_r \cos(\varphi_o - \varphi_r)] \tag{25}$$

where

$$A' = \exp\left[jFA + \frac{j\beta E_0}{2}\right]$$

and

$$\beta = -2FB'$$

Equation (25) has a well known expansion in terms of Bessel functions of the first kind (ref. 26). The first three terms of the expansion are given by

$$T'(\mathbf{r_h}) \sim A'[J_0(\beta t_eU_oU_r) + 2jJ_1(\beta t_eU_oU_r)\cos(\varphi_o - \varphi_r) - 2J_2(\beta t_eU_oU_r)\cos 2(\varphi_o - \varphi_r)] \tag{26}$$

If the argument of the Bessel functions is small and if the variation of the phase factor A' is negligible, then the second term of equation (26) is approximately equal to $j\beta t_eU_rU_o \cos(\varphi_o - \varphi_r)$. The result is a perfect linear recording in the sense of equations (1) and (3).

Even if the argument of the Bessel functions is not small, the phase $\exp j\varphi_o$ still is replicated exactly, and the Bessel function J_1 can be approximated adequately by a linear function of its argument, right up to its first maximum. Hence, it is not surprising that bleached holograms exhibit a linear characteristic over a wide range of exposures and fringe visibilities.

The efficiency for reconstructing the object wave is given by

$$\eta = J_1^2(\beta t_eU_oU_r) \tag{27}$$

where the maximum value is 33.9 percent. This expression is correct for the two-dimensional approximation; higher efficiencies are possible when the thickness of the emulsion is important.

Bleached holograms have several potential sources of noise. The third term of equation (26) is one of a theoretically infinite set of higher orders of diffraction. It reconstructs a wave with a phase $\exp j(2\varphi_o - \varphi_r)$. This wave will not overlap the reconstructed object wave, provided that the off-axis-reference-wave criterion of equation (9) is satisfied. Otherwise, the wave is a potential source of noise. If the argument of the

Bessel functions is chosen to yield an efficiency of 10.8 percent (as calculated from eq. (27)), then J_2^2, the fraction of radiated power in the second term, will be 0.34 percent. The signal-to-noise ratio from the second term alone would be 31 to 1.

The coefficient A' is a phase factor containing a factor proportional to the self-interference term $|O|^2$ which was noted to be a source of noise when the off-axis-reference-wave criterion is not satisfied. That factor can be expanded in the same series represented by equation (26), and the result for the first two terms is

$$\exp \frac{j\ell t_e U_o^2}{2} \sim J_0\left(\frac{\ell t_e U_o^2}{2}\right) + 2jJ_1\left(\frac{\ell t_e U_o^2}{2}\right)$$

The second term introduces self-interference noise. If a beam ratio of 4 (very low) is selected ($U_r/U_o = 2$) and the argument $\ell t_e U_o U_r$ is chosen to yield an efficiency of 10.8 percent, then the fraction of the reconstructed object-wave power which is noise, calculated from

$$\frac{4J_1^2(\ell t_e U_o^2/2)}{J_0^2(\ell t_e U_o^2/2)}$$

is only about 4 percent. The signal-to-noise ratio is then 25. Increasing the beam ratio will reduce this kind of nonlinear noise.

Nonlinear noise in the unbleached hologram will also appear in the bleached hologram. Recall that the second term of the right number of equation (10) represents the first nonlinear term of a silver halide hologram. If that term is significant, then $\ell t_e U_r U_o \cos(\varphi_o - \varphi_r)$ in equation (25) for an ideal bleached hologram must be replaced by

$$\ell\left(1 + \frac{2C'}{B'} t_e U_o^2\right) t_e U_r U_o \cos(\varphi_o - \varphi_r)$$

where C' is the nonlinear coefficient, when exposures are used in place of intensities in equation (10).

With this substitution, the second term of the expansion shown in equation (26) becomes

$$A'\left[2jJ_0(\ell t_e U_r U_o) J_1\left(2\ell t_e^2 \frac{C'}{B'} U_o^2 U_r U_o\right) + 2jJ_0\left(2\ell t_e^2 \frac{C'}{B'} U_o^2 U_r U_o\right) J_1(\ell t_e U_r U_o)\right] \cos(\varphi_o - \varphi_r)$$

Note that A' will contain some other factors as well. The signal-to-noise ratio is now given by the ratio of the square of the second term in the square brackets to the square of the first term in square brackets. For small arguments this ratio is approximately given by

$$\frac{B'^2}{4C'^2 t_e^2 U_o^4}$$

which is the signal-to-noise ratio that would have been calculated for the unbleached hologram.

These various signal-to-noise ratios indicate that the procedure for obtaining a clean reconstructed image is the same as for amplitude modulation holograms. The off-axis-reference-wave criterion should be satisfied, and the beam ratio should be kept as large as possible. A comparatively large reference-wave intensity will keep the product $U_r U_o$ large enough for efficiency, while U_o can be kept small for low noise.

Other sources of noise also seem to be significant to bleached holograms. There is scattering due to surface relief in the emulsion. There is Rayleigh scattering due to refractive index fluctuations in the emulsion. This additional noise is sometimes quite apparent in the reconstructed image. The reconstructed image sometimes appears cleaner, when viewed in the red light of a helium-neon laser, as opposed to the green light of an argon-ion laser. The wavelength dependent scattering is reduced.

The effects of coherence, depolarization, and the use of a diffuser are evaluated in the same way as when an unbleached hologram is recorded. First, the product $U_r U_o$ is replaced by $\sqrt{\psi}\,|\mu|\,U_r U_o$.

The linearity relationship expressed by equation (16) is substituted in equation (23) defining a phase hologram. It is convenient to absorb the impulse response function, the coherence, and the depolarization in an object-wave density, clearly connecting a point on the diffuser with a point on the hologram. When these steps are taken, the phase factor that reconstructs the object wave is given by

$$T'(\mathbf{r_h}) \sim \exp\left[j\ell t_e \int U_r(\mathbf{r_h}) U_o(\mathbf{r_h},\mathbf{r_d})\right] \cos\left[\varphi_o(\mathbf{r_h},\mathbf{r_d}) - \varphi_r(\mathbf{r_h})\right] d\mathbf{r_d}$$

Everything that depends on the coordinate pairs r_h and r_d for the hologram and diffuser, respectively, has been absorbed in the object-wave density $U_o(\mathbf{r_h},\mathbf{r_d}) \exp j\varphi_o(\mathbf{r_h},\mathbf{r_d})$, which interferes with $U_r(\mathbf{r_h}) \exp j\varphi_r(\mathbf{r_h})$ to yield the above expression. One can then show that each diffuser point supplies its own Bessel function expansion at the hologram. Unfortunately, the presence of specular reflections can undo much of the benefit of having correct beam ratios and a correct angle between the diffuser-wave and the reference-wave axes. This problem is discussed in the next section.

Extraneous beams-specular reflections.—A good rule for recording holograms is that only the subject of interest be recorded. Any other light wave can and will degrade the results.

The subject for holography in the flutter cascades was the wave reflected from the back sidewall diffuser. Specular reflections of the object illumination from the windows and

blades are regarded as noise waves. An analysis will be made of the possible consequences of the presence of these noise waves. The analysis is for bleached holograms, although it applies generally to unbleached holograms as well.

The sources of degradation, when an extraneous wave is recorded, are

(1) A reduction of the signal-to-noise ratio, when the extraneous wave overlaps the wave of interest
(2) A reduction of the linear dynamic range and, therefore, the efficiency for recording the wave of interest
(3) The presence of nonlinear noise when the off-axis-reference-wave criterion is not satisfied for the extraneous wave
(4) The presence of noise from the self-interference term of the extraneous wave when the off-axis-reference-wave criterion is not satisfied
(5) The presence of additional nonlinear noise from the extraneous wave when the original silver halide recording has a significant nonlinear term in its transmittance.

For the analysis of these effects, the object wave is conveniently divided into two parts, information wave O_i and a noise wave O_n, where

$$O_i = U_i \exp j\varphi_i \quad \text{and} \quad O_n = U_n \exp j\varphi_n \tag{28}$$

The transmittance of the bleached hologram is proportional, as in the previous section, to a product of exponentials:

$$T \sim \exp\left[\frac{j\beta t_e}{2}(U_i^2 + U_n^2)\right] \exp\left[j\beta t_e U_i U_n \cos(\varphi_i - \varphi_n)\right]$$

$$\exp\left[j\beta t_e U_i U_r \cos(\varphi_i - \varphi_r)\right] \exp\left[j\beta t_e U_n U_r \cos(\varphi_n - \varphi_r)\right] \tag{29}$$

The last two factors in equation (29) predict overlapping noise and information waves, together with a reduction in efficiency for reconstructing the information wave. When the last two factors of equation (29) are expanded, the reconstructed information wave will be proportional to

$$J_0(\beta t_e U_n U_r) j J_1(\beta t_e U_i U_r) \exp j\varphi_i$$

and the reconstructed noise wave to

$$J_0(\beta t_e U_i U_r) j J_1(\beta t_e U_n U_r) \exp j\varphi_n$$

Then the efficiency is given by

$$\eta = J_0^2(\beta t_e U_n U_r) J_1^2(f t_e U_i U_r) \tag{30}$$

The signal-to-noise ratio (ratio of the information-wave intensity to the noise-wave intensity) depends on the place where the waves are detected. At the hologram plane, the ratio is given by

$$\frac{J_0^2(\beta t_e U_n U_r)\, J_1^2(\beta t_e U_i U_r)}{J_0^2(\beta t_e U_i U_r)\, J_1^2(\beta t_e U_n U_r)}$$

For the flutter cascades about 25 percent of the intensity in the overall object waves was extraneous. Suppose that the overall exposure was chosen to yield the maximum efficiency according to equation (27), the efficiency of a bleached hologram. A maximum efficiency of 33.9 percent corresponds to $\beta t_e U_o U_r = 1.84$

Since the information wave is from a diffuser, the information and noise waves are added incoherently (their intensities are added). Their fields on the average are calculated by taking the square roots of their respective intensities. Then $\beta t_e U_i U_r = 1.59$, $\beta t_e U_n U_r = 0.925$, and the efficiency from equation (30) is reduced to 20.5 percent.

The corresponding efficiency for reconstruction of the noise wave is 3.65 percent, so the signal-to-noise ratio is 5.6. This ratio is considerably less than the ratios of 100 or even 25 mentioned previously. Since the object illumination is a diverging beam, the signal-to-noise ratio is even less for photographs of reconstructed images of the blade passages, where the illumination source appears in the photographs.

It is not always possible to avoid recording the specular reflection of the laser source, but viewing that reflection can sometimes be avoided. Still, it is a nuisance, because other effects are present. Equation (30) shows that the efficiency is reduced: The part of the linear range of the emulsion used by the noise wave is wasted. And there are noise contributions, even if the reflections are not viewed directly. Because of the narrow working geometry in the flutter cascades, the off-axis-reference-wave criterion is not satisfied for the specular reflections of the object illumination. Then, as stated in the previous section, nonlinear noise is contributed via J_2 in the Bessel function expansion of the noise-wave exponential. For the reflection from the window, the J_2 contribution is a diverging wave. So its effect on the signal-to-noise ratio is worse in the virtual image than at the hologram.

Also, as stated, the self-interference term of the noise wave makes a contribution to the noise. The self-interference terms appear in the bleached hologram via the first two exponentials of equation (29). Because U_i and O_i are random variables, the second exponential averages to unity. The exponential $\exp j\beta t_e U_n^2/2$ is expanded in a series of some kind, for example, the Bessel function series of the previous section, or simply

$$1 + \frac{j\beta t_e U_n^2}{2} - \frac{\beta^2}{8} t_e^2 U_n^4 + \ldots$$

The powers of U_n increase the divergences of the beams they multiply, including the noise wave itself. The effect can be understood in terms of the setups used to perform

holography in the flutter cascades. To produce the object illumination, the laser beam is split at a 4 percent beam splitter. The 4 percent component is used for the reference beam. The remainder is used as object illumination, since the scattering process at the diffuser is inefficient for illuminating the holographic emulsion. Both beams are diverged by negative lenses. The reconstructed image of the specular reflection of the object illumination is then the image of a point source near the virtual focus of the negative lens. The object illumination can be represented by a Gaussian wave, exactly for the stable resonator and approximately for the unstable resonator. To simplify the argument, it is assumed that the noise wave O_n propagates at a small angle relative to the hologram normal. If the hologram is at a large distance Z_h from the source, then the noise wave is given approximately by

$$O_n = \frac{\exp(-\rho^2/W^2)\exp(-jkZ_h)\exp(-jk\rho^2/2Z_h)}{Z_h} \quad (31)$$

where $\rho^2 = X^2 + Y^2$ (in the hologram plane), $k = 2\pi/\lambda$, and W is called the beam waist, given by

$$W = \sqrt{\frac{b^2 + 4Z_h^2}{kb}}$$

where b is a small quantity determined by the laser and the diverging lens.

Then, the $U_n{}^2$ term is proportional to $\exp -2\rho^2/W^2$. Upon multiplying the noise wave by this factor, a wave is reconstructed proportional to

$$\exp(-3\rho^2/W^2)\exp(-jkZ_h)\exp(-jk\rho^2/2Z_h)$$

The relative divergences of this wave and the noise wave can be compared by using an argument from Fourier optics (ref. 25). At the hologram the process of propagating the Gaussian noise wave is equivalent to placing a transparency, having an amplitude transmittance $\exp(-\rho^2/W^2)$, in contact with a thin lens with transmittance $\exp(-jk\rho^2/2Z_h)$ and focal length Z_h, and illuminating the combination with a plane wave. The process is the same for the wave generated by the self-interference term, except that the amplitude transmittance of the transparency is given by $\exp(-3\rho^2/W^2)$.

This interpretation has the property that, at a distance Z_h from the hologram ($2Z_h$ from the source), the fields will be proportional to the Fourier transformations of the transmittance of the transparencies. The spatial frequency coordinates in the transformation plane are related to the physical coordinates by $F_x = x/\lambda Z_h$ and $F_y = y/\lambda Z_h$.

Without even performing the transformation, the similarity theorem of Fourier transformations can be used to show that the transformation of $\exp(-3\rho^2/W^2)$ and the corresponding light wave are stretched out or scaled by a factor of $\sqrt{3}$ relative to that of the original noise wave; that is the magnitude of the scaled wave is reduced by a factor of 3, and its intensity is reduced by a factor of 9, at corresponding positions. The terms U_n^4, etc., diverge even faster and multiply the information wave, introducing additional noise.

One observable consequence of the divergences of the noise waves is that the signal-to-noise ratio improves as one views the reconstructed image farther from the hologram. Unfortunately, both the field of view and the three-dimensional effect decrease at the same time. Similar effects are introduced by nonlinear terms in the original amplitude-modulation hologram.

Note that the noise waves are beams that can be reflected. Even when angular overlap with a noise wave can be avoided, that wave can still be reflected into the viewing apparatus.

Summary of Single Exposure Holography

The holographic process is affected by a number of factors. The properties of the laser source, its coherence, polarization, and uniformity, have effects entwined with, and similar to, other effects. The performances of both laser sources (stable and unstable) were adequate for the flutter cascade holograms. Further, the holograms could have been improved by precise control of the processing, by using a thinner emulsion, and by eliminating the specular reflections of the object illumination. The only practical step at present is to minimize the effects of the specular reflections (discussed later).

This section has covered the properties of single-exposure holograms. Single exposures here occurred in 15 nsec. The flow visualization technique reported herein depends on double-exposure holograms. The time between exposures is measured in tens of microseconds. Our visualization method makes use of the interference between the two reconstructed waves of the double-exposure hologram. Low signal-to-noise ratios of the individual holograms will decrease the fringe contrast for the two waves. And other effects specifically related to the double-exposure, diffuse illumination method will degrade the fringes. Some of these effects are the same as have been discussed for the single-exposure process, which afterall is a form of interferometry. For example, decorrelation between exposures will reduce the contrast of the interference fringes, just as it reduces the efficiency of the single exposure hologram by reducing the visibility of the hologram. The next main section covers double-exposure, diffuse-illumination interferometry.

Interferometry

Holographic interferometry (the implementation of interferometry using holography) is best summarized in the book by Vest (ref. 27). The present report treats diffuse-illumination interferometry as a three-dimensional flow-visualization technique, rather than as a quantitative technique. The use of double-exposure, diffuse-illumination holographic

interferometry as a three-dimensional flow visualization method has been reported by several authors (refs. 1 to 4). The actual analysis of this method can be quite complex mathematically, so the following review is primarily qualitative.

Review of Diffuse-Illumination Interferometry

The hologram of equation (1) is an example of an interferogram, showing the interference between two scalar waves $O(\mathbf{r})$ and $R(\mathbf{r})$. The interference pattern is a precise encoding of the phase of $O(\mathbf{r})$ relative to that of $R(\mathbf{r})$. The spatial frequencies in the hologram are quite high and not resolvable by the eye.

As an example of an interferogram whose interference-fringe pattern is resolvable by the eye, consider the following. If a double-exposure hologram is recorded, one an exposure of object wave $O_1(\mathbf{r})$ and the other an exposure of object wave $O_2(\mathbf{r})$, the two object waves will be reconstructed independently and simultaneously. The two reconstructed object waves will, in turn, interfere with one another. The interference pattern will be given by

$$I(\mathbf{r}) = |O_1|^2 + |O_2|^2 + O_1^* O_2 + O_1 O_2^* \tag{32}$$

If the difference between O_1 and O_2 is small, the interference pattern will consist of low-frequency interference fringes, easily resolved by the eye. If, however, the difference between O_1 and O_2 is simply a phase shift such that

$$O_2 = O_1 \exp(j\,\Delta\varphi)$$

then the interference pattern is given by

$$I(\mathbf{r}) = 2|O_1|^2(1 + \cos\Delta\varphi) \tag{33}$$

This pattern is said to consist of cosine interference fringes. If O_1 and O_2 represent object waves from two states of a flow field, where the phase change $\Delta\varphi$ is caused by a change in fluid density $\Delta\rho(r)$, then the two are related by

$$\Delta\varphi = K\int \Delta\rho(\mathbf{r})ds \tag{34}$$

where K is a proportiality constant, and where the integral is evaluated along a light ray passing through the fluid. It is most often assumed that the light ray is a straight line (refractionless limit).

In the case of diffuse-illumination interferometry, the phase of O_1 is a radom variable created by passing the object illumination through, or by reflecting it from, a diffuser. An example of a reflecting diffuser is the back sidewall of the flutter cascade (figs. 3 and 4). Ideally, each point in the fluid is illuminated by all points on the diffuser, allowing each point in the fluid to be viewed over a wide angle. Each point in the fluid is imagined to have large pencil of light rays diverging from it.

The phases between different light rays in the pencil are random. But the phase change $\Delta\varphi$ occurring between two exposures along a light ray, is definite. Different light rays do not interfere to produce a low-spatial-frequency interference pattern, resolvable by the eye. However, along each light ray taken by itself, there is an interference corresponding to $\Delta\varphi$.

To view an interference-fringe pattern in diffuse-illumination interferometry, the pencil of light rays diverging from any point in the reconstructed image is reimaged to a point using a lens, for example, the lens of the eye. The cosine interferences of the light rays are superimposed at the imaged point; there is no definite interference between light rays. This is an example of incoherent imaging. The superimposing of the cosine terms of the interferences along individual rays is represented by the sum

$$\sum_i \cos\Delta\varphi_i \tag{35}$$

The summation is over all the light rays in the pencil.

In most cases the phase changes in equation (35) will vary over the entire range from 0 to 2π. Consequently, the sum will tend to zero on average; that is, a typical pencil of light rays from a typical point in the reconstructed image will produce no net interference effect. For some points in the reconstructed image, the phase changes $\Delta\varphi$ may vary slowly enough over a pencil that an interference effect is perceived. The point observed is then called a point of localization. For a particular viewing direction, or viewing axis, through a point, localization will occur (or is defined to occur) when

$$\frac{\partial\Delta\varphi}{\partial\theta x} = 0 \quad \text{and} \quad \frac{\partial\,\Delta\varphi}{\partial\theta y} = 0 \tag{36}$$

The variations in viewing direction are given by the angles θ_x and θ_y. The angle θ_x is zero along the viewing axis, and represents a variation of light-ray direction in a plane containing the viewing axis and the x axis. Similarly, θ_y is zero along the viewing axis, and represents a variation of light-ray direction in plane containing the viewing axis and the y axis. For simplicity, both the diffuser and hologram are assumed to be parallel to the xy plane.

Localization occurs for sets of points in the neighborhoods of curves or surfaces (refs. 3, 4, and 27). It is on or near these curves or surfaces that interference fringes appear to be located in the reconstructed image. The process of viewing localized fringes in the reconstructed image of a double-exposure hologram is shown schematically in figure 9.

The phenomenon of fringe localization is used for three-dimensional flow visualization of flow features as follows. If a flow feature has a small spatial extent along the viewing direction and, also, a large gradient of density transverse to the viewing direction, then the interference fringes will localize

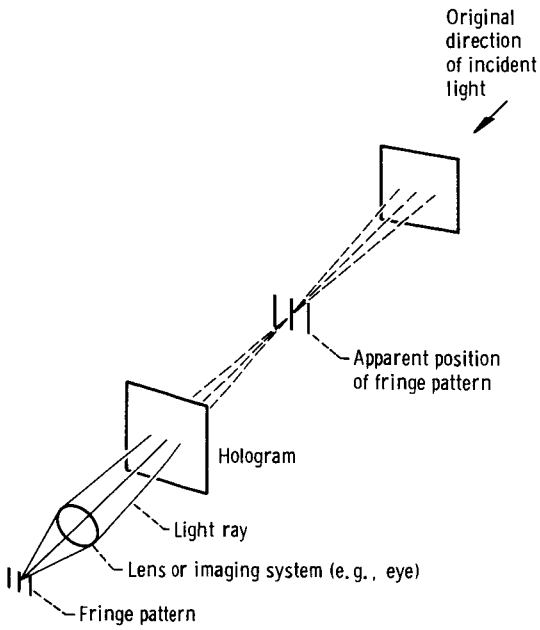

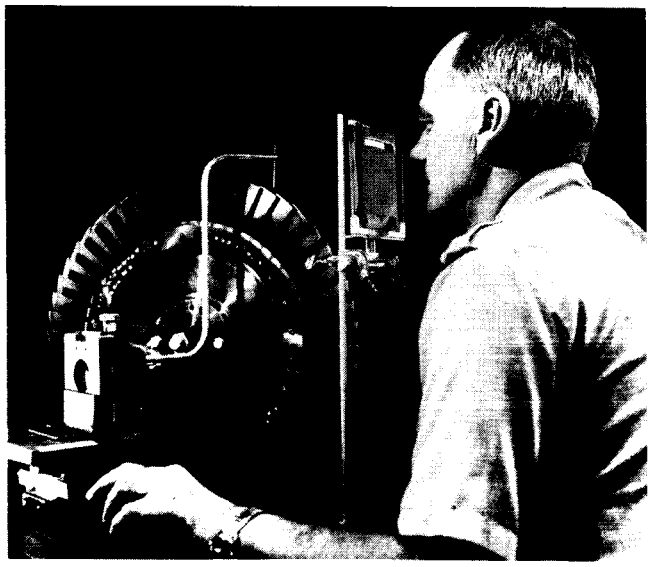

Figure 9.—Imaging and viewing a localized interference-fringe pattern.

nearby, on, or within the flow feature. In a sense the interference fringes are painted on the flow feature making it visible. In the reconstructed images shown in figure 5, the hair-like structure or filaments are interference fringes localized on the shock-wave positions. If a flow feature has a large extent but is symmetrical about the viewing direction, the fringe pattern tends to localize midway in the feature.

A shock-wave surface viewed close to tangency is a limiting case of a flow feature having a small extent along the viewing direction and a substantial density gradient transverse to the viewing direction. The influences of its strength, curvature, and viewing angle on localization have been calculated by Decker (ref. 3). Schumann (ref. 28) has pointed out that, in general, best localization and visualization of a transparent subject will occur when the viewing direction is perpendicular to the gradient of the refractive index.

This concludes this brief review of the fundamentals of diffuse-illumination, holographic interferometry as a three-dimensional flow visualization technique.

Defects of the Interferometric Process

The defects of the interferometric process as an imaging or visualization technique are similar to those of the holographic process. A defective interference fringe pattern has low contrast. It may also be difficult to associate with, or localize on, a particular flow feature. Defects of the visualization process are associated with

(a) Poor view of a flow feature
(b) Sign changes in the gradient of the change in density
(c) Flow-feature interferences
(d) Poor hologram
(e) Motion of the holographic setup between exposures
(f) Exposure variations between pulses of a pulse pair
(g) Aberrations.

Not included for discussion are real flow features that are undesirable, annoying, or confusing to a casual observer, but do not represent a defect of the visualization process. A method for enhancing the visualization of a particular flow feature is suggested later.

Good visualization requires that the interference fringes have high contrast and that the contrast decreased rapidly, when the fringes are viewed away from the surfaces or curves of localization. Since the concepts of visibility and contrast are quite important in discussing three-dimensional visualization based on interferometry, these concepts are reviewed below.

Visibility and contrast.—The interference-fringe visibility V has been defined in terms of the local maximum and minimum intensities I_{max} and I_{min}, where

$$V = \frac{I_{max} - I_{min}}{I_{max} + I_{min}} \tag{37}$$

The subjective viewing of patterns is often discussed in terms of contrast $\mathcal{C}$. There is an objective definition of contrast. That definition will be modified shortly, but it is given by

$$\mathcal{C} = \frac{I_{max} - I_{min}}{I_{min}} = \frac{2V}{1 - V} \tag{38}$$

Interpreting intensity as an observable quantity is somewhat difficult. The intensity can be regarded as the maximum power per unit area in the electromagnetic field, without regard for the directions of propagation of the electromagnetic modes. It can be identified with the magnitude of the Poynting vector.

For subjective viewing of a pattern, photometric quantities are used. The intensity is replaced by the luminance L where

$$\mathcal{C} = \frac{L_{max} - L_{min}}{L_{min}} \tag{39}$$

In the most general case, L_{max} and L_{min} do not even have to refer to the same colors. That case does not occur with single-frequency laser light. For the laser illuminated diffuser, the following definition of luminance is used. The luminance L is the power per unit area at the pupil of the eye, divided by the solid angle subtended by the diffuser at the pupil and multiplied by the luminosity factor corresponding to the laser wavelength. If it is assumed that the entire diffuser fills the field of view of the eye, then the luminance does not change with the distance from the diffuser. The luminosity factor depends on whether rods or cones are being used for viewing. When cones are used for color vision, the luminosity factor for the 532 nm wavelength (should it be used for reconstruction) is about 580 lm/W. The factor at 633 nm is about 170 lm/W.

Because relative values are used to calculate contrast and because single-frequency, visible laser light was used, it is assumed that either equation (38) or (39) will yield the subjective contrast. It should be noted that viewing the interference fringes directly, with a film or TV camera, yields different results. The slope of the characteristic of the viewing device has a significant effect on the perceived results. Generally, a high contrast imaging device such a silicon-target vidicon makes it easier to view the flow features reconstructed from the flutter cascade holograms, than to view them with the eye, for example.

The contrast has an interesting interpretation, provided that certain assumptions are satisfied. If I_{min} or L_{min} is due to noise waves only and if the noise and signal waves are mutually incoherent, then the contrast is identical with the signal-to-noise ratios discussed previously. Identifying $\mathcal{C}$ with the hologram signal-to-noise ratio is generally not a correct procedure, because the signal and noise waves may be coherent. However, some feeling for what the signal-to-noise ratios mean can be had by temporarily making this identification.

In one experiment (ref. 29) it was determined that an object in background illumination could be recognized with 95 percent certainty, when $\mathcal{C} = 1$. In this experiment an object was viewed with flashed illumination. So this threshold value of $\mathcal{C}$ is probably larger than would be measured with steady illumination.

The conclusion is that a signal-to-noise ratio of unity leads to possible, but difficult, viewing. For the signal-to-noise interpretation of $\mathcal{C}$, very good holograms have $\mathcal{C} = 100$. For bleached holograms, the contrast $\mathcal{C}$ ranges from 10 to 30, provided that there are no noise waves.

Next, the visibility and the contrast are derived for the simplest conditions under which fringes are formed in diffuse-illumination interferometry. Additional explanations are provided for the differences between diffuse-illumination and ordinary interferometry.

Basic visibility and contrast of diffuse-illumination fringes.—The fringe pattern observed in diffuse-illumination interferometry is a function of the imaging system. It does not exist without the optical system used to view it. In this sense, diffuse-illumination interferometry is very different from ordinary interferometry, wherein the fringe pattern is a fundamental property of the electromagnetic field. The interference pattern, for mutually coherent light beams, exists everywhere that the light beams overlap.

On the other hand, the perception of fringes in diffuse-illumination interferometry is strictly an incoherent imaging process. (The interference of the two reconstructed light waves, leading to definite interference along a light ray, is still a coherent effect.) Light rays passing through a point in the virtual image of the double-exposure hologram are reimaged at a point by the eye (or any lens). When the patterns along different ray directions overlap in registration, then a fringe pattern is perceived. In this sense the morphology of the patterns detected in diffuse illumination interferometry is similar to that of patterns such as the stripes of a tiger or moire fringes. Diffuse-illumination interferometry is an incoherent way of observing a coherent effect.

Specifically, along each light ray through a point in the virtual image, there is a definite (as opposed to stochastic) interference between the two exposures, where

$$dI = [U_1^2 + U_2^2 + 2U_1U_2 \cos(\Delta\varphi)]dx\,dy \tag{40}$$

Note that each light ray is associated with a small area $dx\,dy$ on the diffuser. There is a certain minimum area, depending on the resolution of the imaging system, over which the light in the image is spatially coherent. Equation (40) for a single light ray expresses a coherent effect.

The summation of the light rays at the image point at the retina of the eye, the film of a camera, or any other imaging device is an incoherent addition of the light-ray intensities where

$$I = \int[U_1^2 + U_2^2 + 2U_1U_2 \cos(\Delta\varphi)]dx\,dy \tag{41}$$

No noise has been included in equation (40). No incoherence effects between the two exposures along the same light ray have been included. The integral is over the base of the cone or pencil of light rays, intersecting the diffuser. The apex of the cone or pencil is the point in the virtual image which is reimaged by the imaging device.

If dI does not depend on the ray direction in the pencil of rays, then the integral has a simple evaluation, where

$$I = 4\,\Delta x\,\Delta y\left[U_2^2 + U_2^2 + 2U_1U_2 \cos(\Delta\varphi)\right] \tag{42}$$

Here, the rectangular format for the projection of the pencil of rays is retained. The half projections of the pencil of rays about the optical axis of the imaging system are Δx and Δy. The visibility depends on the beam ratio, as in holography, and is given by

$$V = \frac{2U_1U_2}{U_1^2 + U_2^2} \tag{43}$$

From equation (38), the contrast $\mathcal{C}$ is given by

$$\mathcal{C} = \frac{4U_1U_2}{(U_1 - U_2)^2} \tag{44}$$

Since the term "visibility" is usually reserved for coherent interference effects, we might call V in equation (43) the pattern modulation, or something else. But visibility is used in this report.

If $\Delta\varphi$ varies as function of the ray direction in the pencil, then the calculation of the visibility or contrast is slightly more complex. Said variation is the common case and leads to localization. In one argument (ref. 27), the ray along the optical axis is identified with the intersection point x_0y_0 at the diffuser.

Then, $\Delta\varphi$ is expanded to first order about this intersection point to vary the ray direction over the pencil. This expansion is given by

$$\Delta\varphi(x,y) = \Delta\varphi(x_0,y_0) + \frac{\partial\,\Delta\varphi}{\partial x}(x - x_0) + \frac{\partial\,\Delta\varphi}{\partial y}(y - y_0) \tag{45}$$

If the localization conditions of equation (36) are satisfied, then, to first order, the change in phase does not vary over the pencil of rays, and equations (42) to (44) are valid. Best visibility and contrast occur for $U_1 = U_2$. (In fact, this may not be the case for a nonlinear recording material like a silver halide emulsion. Equal exposures can yield holograms with different reconstruction efficiencies.)

When the localization conditions are not satisfied, the visibility and contrast decrease, as they should. When equation (45) is substituted into equation (41), the intensity at the imaged point is given by

$$I = 4\,\Delta x\,\Delta y[U_1^2 + U_2^2 + 2\gamma U_1U_2\cos(\Delta\varphi(x_0,y_0))] \tag{46}$$

where (ref. 27)

$$\gamma = \frac{\sin\left(\frac{\partial\,\Delta\varphi}{\partial x}\Delta x\right)\sin\left(\frac{\partial\,\Delta\varphi}{\partial y}\Delta y\right)}{\left(\frac{\partial\,\Delta\varphi}{\partial x}\Delta x\right)\left(\frac{\partial\,\Delta\varphi}{\partial y}\Delta y\right)}$$

Again, the maximum value of γ is unity when the localization conditions are satisfied. For the cosine fringe pattern of equation (46), the visibility is given by

$$V = \frac{2\sqrt{P}\,\gamma}{1 + P} \tag{47}$$

where P is again a beam ratio,

$$P = U_1^2/U_2^2 \quad \text{or} \quad P = U_2^2/U_1^2$$

Equation (47) is like equation (13) for the fringe visibility for holograms. The contrast $\mathcal{C}$ is given by

$$\mathcal{C} = \frac{4\sqrt{P}\,\gamma}{1 + P - 2\sqrt{P}\,\gamma} \tag{48}$$

As the condition for localization is violated, γ, V, and C all decrease. A criterion can be proposed for the scene depth, the depth perpendicular to the diffuser over which the contrast is high enough for a pattern to be perceived. Let the beam ratio P be unity. Recall that $\mathcal{C} = 1$ was given as a criterion for least visible fringes. When $\mathcal{C} = 1$, then $\gamma = 0.333$; and we could define the scene depth as the distance between contrast values of unity. However, it is more convenient to let, and there is little difference in letting, the contrast $\mathcal{C}$ and γ go all the way to zero in defining the scene depth. The scene depth is then the range of distance, perpendicular to the diffuser, where

$$\left.\begin{aligned} -\pi/\Delta x < \partial\,\Delta\varphi/\partial x < \pi/\Delta x \text{ or} \\ -\pi/\Delta y < \partial\,\Delta\varphi/\partial y < \pi/\Delta y \end{aligned}\right\} \tag{49}$$

For a particular flow feature, it is algebraically complicated to calculate the surfaces of localization and the scene depth. The somewhat singular case of shock-wave surfaces is treated in references 3 and 4. The relationship between the flow-field density distribution and fringe localization is reviewed, next.

Flow-density field and localization.—A simplification, adopted in this paper, is that the view is nearly normal to the diffuser. This is the case in the flutter cascades. In place of density, the refractive index field is used. The two quantities are proportional.

For this simplified case, reference 3 yields the following forms for equations (36):

$$\left.\begin{aligned} \frac{\partial\,\Delta\varphi}{\partial x} = \frac{2\pi}{\lambda}\int\frac{\partial f}{\partial x}\,dz - \frac{1}{Z}\int\frac{\partial f}{\partial x}z\,dz = 0 \\ \frac{\partial\,\Delta\varphi}{\partial y} = \frac{2\pi}{\lambda}\int\frac{\partial f}{\partial y}\,dz - \frac{1}{Z}\int\frac{\partial f}{\partial y}z\,dz = 0 \end{aligned}\right\} \tag{50}$$

where the angular variations in equations (36) have been parameterized by the ray intersection coordinates, x and y, where f is the change in refractive index between the two

exposures of the double-exposure hologram, and where Z is the perpendicular distance of localization, measured from the diffuser.

Then, for a nearly normal view of the diffuser, localization is given by

$$\left.\begin{aligned} Z &= \frac{\int \partial f/\partial x\, z\, dz}{\int \partial f/\partial x\, dz} \\ Z &= \frac{\int \partial f/\partial y\, z\, dz}{\int \partial f/\partial y\, dz} \end{aligned}\right\} \tag{51}$$

The integrals are evaluated over the range of z where the derivatives of the change in refractive index (or density) are significant.

Localization is given by two equations (51), which express Z as a function of x and y. Hence, each equation is a surface, and localization occurs, in general, on a geometrical curve. For a correct choice of the x and y axes in the diffuser, it often happens that one of the equations (36) or (50) is satisfied in the trivial sense. Then, one of equations (51) applies, and localization is on a surface.

Equations (36), (50), and (51) assume that the rays within the cone or pencil can be varied independently and simultaneously in two directions. If a slit is used to confine this variation to one direction only, then one equation determines localization, and localization is on a surface. Slit viewing is often the most desirable way to view a diffuse-illumination interferogram: It maximizes contrast over a larger area transverse to the viewing direction. In viewing the flutter-cascade holograms, slit viewing sometimes sharpens the visualization noticeably. These comments emphasize how much diffuse-illumination fringes depend on the incoherent imaging properties of the imaging system.

Localization is observed in equations (51) to be a weighted sum of positions, where the weighting factor is the normalized transverse gradient of the change in refractive index. Only in special cases are the equations (50) and (51) likely to predict good three-dimensional flow visualization. This fact must be considered in evaluating the overall performance of the holographic system used in the flutter cascades. In the next section some of the properties of a suitable subject for visualization are presented, and two defects of the visualization process are discussed.

Localization defects and feature interferences.—In general, the flutter-cascade flows provided excellent views of the shock waves, but the views suffered from turbulent-boundary-layer interferences. The effects of the views on localization and the effects of the interferences are discussed in this section.

Flow features can be classified in order of their suitability for three-dimensional visualization. The most suitable subject is an isolated feature, of small extent, whose presence is negligible during one of the two exposures of the double-exposure hologram and for which $\partial\rho/\partial x$ has a single sign (either positive or negative) along the line of sight. Only the x formulas are listed, since the y formulas have identical forms.

Then, the interference pattern from equation (34) is given by

$$\Delta\varphi = K\int(\rho - \rho_0\, dz) \tag{52}$$

where ρ_0 is the slowly varying density in the absence of the flow feature.

The variation of the phase corresponding to equations (50) is given by

$$\frac{\partial\, \Delta\varphi}{\partial x} = K\left(\int \frac{\partial\rho}{\partial x}\, dz - \frac{1}{Z}\int \frac{\partial\rho}{\partial x}\, z\, dz\right) \tag{53}$$

and localization is given by

$$Z = \frac{\int \partial\rho/\partial x\, z\, dz}{\int \partial\rho/\partial x\, dz} \tag{54}$$

For example, equations (52) to (54) apply when a flow versus no-flow comparison is made, when a flow feature moves into a previously quiescent region, or when the strength of a flow feature changes substantially between exposures. Shock-wave-surface visualization is best accomplished with this mode.

A less suitable, but still useful, subject is a strong, isolated feature, of small extent, which moves a small x-distance between exposures of a double-exposure hologram, and for which $\partial^2\rho/\partial x$ had a single sign (either positive or negative) along the line of sight. Then, to first order in the density as a function of x

$$\Delta\varphi = -Ka\int \frac{\partial\rho}{\partial x}\, dz \tag{55}$$

The variation of the phase is given by

$$\frac{\partial\, \Delta\varphi}{\partial x} = -Ka\left(\int \frac{\partial^2\rho}{\partial x^2}\, dz - \frac{1}{Z}\int \frac{\partial^2\rho}{\partial x^2}\, z\, dz\right) \tag{56}$$

and localization is given by

$$Z = \frac{\int \partial^2\rho/\partial x^2\, z\, dz}{\int \partial^2\rho/\partial x^2\, dz} \tag{57}$$

For both of these first two modes, localization occurs within the flow feature. If the flow feature is symmetrical about a plane parallel to the xy plane, then localization occurs within the plane of symmetry. The feature can be accurately located within the flow passage.

The scene depth (depth-of-field) can be calculated using equation (49) and equations (53) or (56). For the first mode the scene depth is given by

$$\Delta = \left(\frac{Z}{2\,\Delta x}\right)\left(\frac{4\pi}{K\int \partial\rho/\partial x\,dz}\right) \tag{58}$$

and for the second mode

$$\Delta = \frac{Z}{2\,\Delta x}\,\frac{4\pi}{-Ka\int \partial^2\rho/\partial x^2\,dz} \tag{59}$$

The factor $Z/2\,\Delta x$ is the angular aperture of the imaging system, as measured from the point Z of localization. A feeling for localization on a turbulent eddy in a boundary layer can be developed from equation (59). The feature is taken to be spherically symmetrical with a density that differs from that of its surroundings according to

$$\left.\begin{aligned} \rho &= \rho_0\left(1-\frac{r^2}{r_0^2}\right) \qquad r < r_0 \\ \rho &= 0 \qquad\qquad\qquad \text{otherwise} \end{aligned}\right\} \tag{60}$$

Then

$$\partial^2\rho/\partial x^2 = -\frac{2\rho_0}{r_0^2} \tag{61}$$

If equation (61) is substituted into equation (57) for localization, it is observed, as expected, that localization occurs in the plane $Z = Z_0$, where Z_0 is the z-coordinate of the center of the sphere.

When equation (61) is substituted into equation (59) for the scene depth, or depth-of-field, the depth is given by

$$\Delta = \left(\frac{Z_0}{2\,\Delta x}\right)\left(\frac{\pi r_0^2}{k\rho_0 a\delta}\right) \tag{62}$$

where 2δ is the length of the segment of the light ray intersecting the sphere.

The turbulence in the flutter cascades is assigned the following properties: The view is selected through the center of the sphere so that $\delta = r_0$. The coefficient K is given by $K = 2\pi G/\lambda$, where G is the Gladstone-Dale constant. For air and for $\lambda = 0.532\times10^{-6}$ m, $G = 0.227\times10^{-3}$ m^3/kg and $K = 2.68\times10^3$ m^2/kg.

The sphere diameter is assigned a value equal to the thickness of the boundary layer of 1 cm. Hence, $\mathbf{r} = 0.005$ m. The velocity at midboundary layer is about 237 m/sec, so the distance moved in a typical 15 μsec interexposure time is given by $a = 3.56\times10^{-3}$ m. The value of the density is estimated by making it identical with the maximum density variation within the boundary layer, $\rho_0 = 0.0870$ kg/m^3. When these values are substituted into equation (62) and a viewing aperture of 10 is selected, the scene depth is found to be about 20 cm.

The turbulence is generally poorly localized within the flow passage, which has a span width of about 10 cm. As the view deviates from the center of the sphere, the localization deteriorates inversely as δ. The localization is also poorer for smaller values of the density variation and the interexposure displacement a. When the turbulence in the reconstructed images of the flutter cascade flows is viewed, much of the turbulence appears to be impressed on the diffuser. The eye evidently prefers to lock onto a diffusely reflecting surface in the absence of good localization. It should be mentioned that well-localized turbulent-like features were observed in some of the reconstructed images. For these features the implication is that r_0 is smaller, or that ρ_0 and a are larger, than used in the above example.

A flow feature is much less suitable for visualization, if the derivatives of density change sign along the line of sight. One defect is that localization does not necessarily occur within the flow feature; then there is a localization error. Another is that cancellation within the integrals of equations (58) or (59) increases the scene depth, thereby reducing the sharpness of the three-dimensional view. In same cases the derivatives of density can be absolutely large, yet the localization poor. The calculation of localization becomes ill-posed also.

One example of this defective (but at times necessary) form of diffuse illumination interferometry is the so-called rapid-double-exposure technique for shock-wave-surface visualization. The technique is explained in detail in references 2 and 3. In that technique the shock wave is allowed to move slightly between the two exposures of the double-exposure hologram. A light ray intersects the shock wave twice, once at each exposure. The defect in this procedure is that the contributions to the localization integrals at the two intersection points enter with opposite signs. The user is entirely dependent for localization on the shock wave having different properties at each of the two intersection points. Then, cancellation is not complete.

The properties of a shock-wave surface that vary spatially are the orientation and the strength. The orientation varies more rapidly if the shock wave is curved. The spatial separation between the intersection points and the light ray can be increased by viewing the shock wave close to tangency.

In some cases all attempts to promote localization using the rapid-double-exposure method may fail. Then it is necessary to view the shock-wave surface so close to tangency that only one intersection between a light ray and the shock wave occurs. The visualization technique is that of the first mode. The angular range for a single intersection can be increased as one approaches a boundary layer. The flutter cascade images are easiest to view near the end-wall boundary layers.

One difficulty in viewing the shock waves in the flutter cascades was possibly due to localization interferences with the boundary-layer turbulence. If there is an overlap of two features along the line of sight, the interference fringes do not

necessarily localize on either feature. The localization surfaces may be spatially complex and not easily related to either feature. To a considerable extent, the flutter cascade holograms were evaluated in terms of their ability to display three-dimensional images of the shock waves. Frequently, the shock waves were viewed against a background of end-wall boundary-layer turbulence, particularly in the case of the larger flutter cascade. The effect of this mode of viewing is now estimated.

Mainly because of the complexity of performing the following estimates for rapid-double-exposure holography of the shock waves, it is assumed that the shock wave is viewed by means of the single-ray intersection. In the flutter cascades the views could be made as close to tangency as desired. The light ray is also assumed to pass through a turbulent eddy (modeled by eq. (60)). The localization equation then assumes the form

$$Z = \frac{\int_{\text{shock}} \partial\rho/\partial x\, z\, dz - a \int_{\text{eddy}} \partial^2\rho/\partial x^2\, z\, dz}{\int_{\text{shock}} \partial\rho/\partial x\, dz - a \int_{\text{eddy}} \partial^2\rho/\partial x^2\, dz} \tag{63}$$

The scene depth, in turn, is given by

$$\Delta = \frac{4\pi}{\int_{\text{shock}} \partial\rho/\partial x\, dz - a \int_{\text{eddy}} \partial^2\rho/\partial x^2\, dz} \frac{Z}{2\ \Delta x\ K} \tag{64}$$

Note that the localization integrals of overlapping features are added in series, where each integral is selected according to the particular mode of visualization.

In the flutter cascades, the shock waves, can be represented in part, by the following model. The shock wave is a plane surface whose normal is nearly along the x axis in the xz plane. The shock wave is represented by the equation

$$z = x \tan\theta$$

where the angle θ approaches 90°. This model represents the shock waves away from the blades. The change in density across the shock wave is called ρ_s. Then (from ref. 3) the derivative of the density, in the x direction, has the following limiting form at the shock-wave surface:

$$\frac{\partial\rho}{\partial x} = \rho_s(\tan\theta)\delta(x \tan\theta - z) \tag{65}$$

where δ here represents the Dirac delta function. The integrals involving x are easily evaluated because of the delta function, and are given by

$$\int \frac{\partial\rho}{\partial x} dz = \rho_s \tan\theta \tag{66}$$

$$\int \frac{\partial\rho}{\partial x} z\, dz = \rho_s x \tan^2\theta \tag{67}$$

In the absence of the eddy, the quotient of equations (66) and (67) yields localization precisely on the shock wave at $Z = x \tan\theta$. The scene depth or depth-of-field in the absence of the turbulent eddy is given by equation (58) as

$$\Delta = \frac{Z}{2\ \Delta x} \frac{4\pi}{k\rho_s \tan\theta}$$

Since $\tan\theta$ can be selected to be arbitrarily large, localization can be arbitrarily precise.

Now suppose that the ray also passes through the eddy. Localization is determined by substituting equations (61), (66), and (67) into equation (63). The result is given by

$$Z = \frac{x \tan\theta + \dfrac{4\rho_0 a Z_0 \delta}{r_0^2 \rho_s \tan\theta}}{1 + \dfrac{4\rho_0 a\delta}{r_0^2 \rho_s \tan\theta}} \tag{68}$$

Again, by making $\tan\theta$ large enough, localization (due to the x-equation) occurs at the shock wave. The scene depth, due to x-equation (64), is given by

$$\Delta = \frac{\dfrac{Z}{2\ \Delta x} \dfrac{4\pi}{K\rho_s \tan\theta}}{1 + \dfrac{4\rho_0 a\delta}{r_0^2 \rho_s \tan\theta}}$$

The scene depth, due to the x-variation, can be made as small as desired by making $\tan\theta$ large enough.

If the x-equations are soley responsible for localization, the only effect of turbulence would be to reduce slightly the range of angles over which the shock wave could be viewed sharply. Unfortunately, unless the y view is restricted, the y-equations also determine localization. And the y-equations are determined entirely by the turbulent eddy; the shock wave contributes no y-derivatives of density.

A consequence is that the shock wave will be visible with high contrast only within one eddy-determined scene depth of the eddy. This scene depth is large for much of the turbulence. However, there are features for which it is small.

Even when the scene depth is large, the turbulence reduces the contrast (signal-to-noise) of the shock-wave fringe pattern. As the shock wave is viewed through different parts of the eddy, through different eddies, between eddies, and with varying restrictions on the y-view, the quality of the shock-wave visualization varies considerably.

The random nature of the boundary layer turbulence creates a frame-to-frame variation in the quality of the shock-wave visualization. This effect can be seen in figure 10, where all frames were recorded at the same blade angle of attack.

The boundary layer turbulence complicates the interpretation of the holograms in terms of shock-wave visualization. If the turbulence cannot be eliminated, it can be minimized by using as short an interexposure time as possible, thereby reducing the parameter a in the localization equations. Another possible minimization technique, using time-average holography, is suggested later.

Finally, some other influences on interference-fringe contrast and visibility are summarized next.

Hologram noise.—Contrast degradations due to localization problems and feature interferences have been discussed for an ideal holographic process. For such a process, the maximum contrast at a point of localization is determined by the beam ratio $P = U_2^2/U_1^2$. When $P = 1$, then $\mathcal{C} = \infty$ and $V = 1$. The actual maximum contrast and its positional variation are affected by hologram noise, diffuser motion, window motion, fluctuations in the reconstructed beam ratio, and third-order aberrations. First, consider hologram noise.

Let the noise be incoherent with the two object waves O_1 and O_2. If the noise along a light ray intersecting the diffuser at (x,y) is called $N(x,y)$, then equation (41) for the intensity at an image point is modified to be

$$I = \iint [N(x,y) + U_1^2 + U_2^2 + 2U_1U_2 \cos(\Delta\varphi)]\,dx\,dy \tag{70}$$

If the noise is expanded to first order about the optical-axis, which intersects the diffuser at (x_0,y_0), then the intensity becomes

$$I = 4\,\Delta x\,\Delta y\,N(x_0,y_0) + \iint [U_1^2 + U_2^2 + 2U_1U_2 \cos(\Delta\varphi)]\,dx\,dy$$

When the localization criterion is applied, equation (42) assumes the modified form

$$I = 4\,\Delta x\,\Delta y\left[N(x_0,y_0) + U_1^2 + U_2^2 + 2U_1U_2 \cos(\Delta\varphi)\right] \tag{71}$$

Assuming either that the noise is constant or varies rapidly in comparison with the variation of the fringe pattern allows the visibility from equation (71) to be given by

$$V = \frac{2U_1U_2}{N(x_0,y_0) + U_1^2 + U_2^2} \tag{72}$$

and the contrast is given by

$$\mathcal{C} = \frac{2U_1U_2}{(U_1 - U_2)^2 + N(x_0,y_0)} \tag{73}$$

In other words, the hologram noise affects the fringe contrast and, thereby, the visualization quality in exactly the same way that it affects the single-exposure image quality. The three-dimensional fringe pattern behaves like a three-dimensional object in all respects.

Diffuser motion and window motion.—Because of the long interexposure times, diffuser motion is more likely to be a problem in double-exposure than in single-exposure holography. Again, there are two kinds of motion-related degradation: fringes caused by diffuser motion, principally along the viewing direction, and a reduction in fringe contrast due to decorrelation.

If the diffuser twists about the y-axis and if the illumination and viewing directions are nearly normal to the diffuser, fringes form nearly in the plane of the diffuser and parallel to the y-axis. If a flow object is also present, localization equations (51) become

$$Z = \frac{\int \partial f/\partial x\, z\, dz}{\int \partial f/\partial x\, dz + \partial\delta/\partial x} = \frac{\int \partial f/\partial y\, z\, dz}{\int \partial f/\partial y\, dz} \tag{74}$$

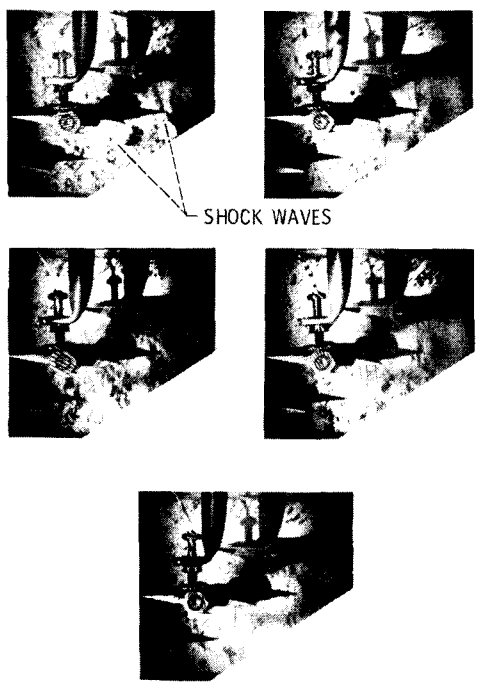

Figure 10.—Frames from holographic motion picture of shock waves in a three-blade flutter cascade. All frames recorded at the same blade angle of attack.

where δ is the diffuser displacement, as a function of distance from the y-axis. Hence, for a twist, $\partial\delta/\partial x$ = constant. The localization equation in the y-direction is unaffected, but the localization equation in the x-direction tends to pull localization toward the diffuser. Again, a shock wave, whose normal is nearly along the x-direction, can be made to dominate this integral.

Rigid motion of the diffuser along the viewing direction produces fringes that tend to localize at infinity. If there is a flow object present and if the illumination and viewing directions are nearly normal to the diffuser, then the localization equations become

$$Z = \frac{\delta + \int \partial f/\partial x \, z \, dz}{\int \partial f/\partial x \, dz} \qquad (75)$$

$$Z = \frac{\delta + \int \partial f/\partial y \, z \, dz}{\int \partial f/\partial y \, dz}$$

Because δ is small, localization will hardly be affected by rigid motion of the diffuser along the viewing direction. In any case, no evidence of a large twist of the diffuser was observed in the reconstructed images.

A more likely possibility is significant motion along the flow passage, resulting in motion in the plane of the diffuser. This motion will cause decorrelation. Decorrelation will cause a reduction in fringe contrast.

The fringe visibility is reduced by a factor that is dependent on the effective F/number of the viewing system. If there is a transverse displacement, δ, between exposures, then the fringe visibility is reduced by the factor

$$\mu = \frac{2J_1(\pi\delta/F\lambda)}{(\pi\delta/F\lambda)} \qquad (76)$$

This factor has its first zero at a value of δ corresponding to the Rayleigh criterion resolution of the viewing system. The first zero occurs when

$$\delta = 1.2 \, F\lambda \qquad (77)$$

Motion can be compensated for by increasing the F/number, but the three-dimensional viewing effect will decrease. Some of the frame-to-frame variation in hologram image quality may have been caused by transverse motion of the diffuser.

The windows used were schlieren quality, but not interferometer quality. The effects of window motion would be the same as the effects of a time varying flow. For the best results, it is recommended that the velocities of the window and diffuser be monitored. Holograms would be recorded during low velocity conditions. It is also recommended that interexposure times be 15 μsec or less for the best results.

Beam ratio fluctuations.—The beam ratio $P = U_2^2/U_1^2$ can be held to about a ± 20 percent variation. At the extremes the fringe contrast is reduced to $C = 20$. Having a beam ratio at the extremes is equivalent to introducing any of a number of hologram noise sources. Should there be larger variations in the beam ratio, for example, because the Q-switch of the laser malfunctions, the contrasts of some of the images will be even less. If the illumination profile changes between the pulses of a pulse pair, the beam ratio will fluctuate. It is recommended that the repeatability of the properties of the laser beam, between pulses of a pulse pair, be carefully specified and verified.

Aberrations.—The interference fringe pattern is affected by the third-order hologram aberrations in exactly the same way that a single-exposure image is affected (as discussed in ref. 3). These aberrations occur when the wavelength or geometry of the reconstruction beam differs from that of the reference beam. The aberrations can reduce the fringe contrast. But the previously considered effects seem to be much more significant.

Summary of interferometry for flow visualization.—The laser system used cannot compensate for a failure to meet the principal requirement for good three-dimensional flow visualization based on diffuse-illumination interferometry. That requirement is the selection of a suitable flow field and the correct view of that flow field. The objective is to achieve good localization on individual flow features and to avoid flow feature interferences.

Having satisfied the principal requirement, the objective next is to minimize degradation of the fringe contrast due to hologram noise and motion of the optical components of the holography setup.

The laser will have a significant negative effect on the results, if the reconstructed beam ratio cannot be maintained near unity. The two pulses radiated by the laser during a double exposure should be as nearly identical as possible.

Results and Discussion

The experimental history of Nd:YAG holography in the flutter cascades and the analysis of holography and interferometry, reported herein, are summarized in this section. The results suggest how holographic systems of the kind discussed might be constructed and operated and how the results might be interpreted.

One result of the analyses of holography and interferometry was the establishment of a reasonable objective for diffuse-illumination, holographic interferometry in a flow facility. The objective established was to achieve a brightly reconstructed image of a fringe, with a contrast factor or signal-to-noise of 10 to 20. To achieve this objective, it was essential to eliminate specular reflections or to reduce their effects. There are three approaches.

If the angle of incidence of the object illumination can be made large enough, then the window-reflection of the object

illumination will miss the hologram. This approach was not possible in the flutter cascades.

Another approach is to place the effective source for illuminating the object at a large distance from the test section. The object illumination can be collimated or coveraged slightly. However, the useful linear dynamic range will still be less than the maximum.

A final approach is simply to avoid recording a hologram of the specular reflections, even when they reach the hologram. If the object illumination is polarized at 90° to the polarization of the reference beam, then holograms of the specular reflections are not recorded. To record a hologram of the diffuser, as desired, it was necessary to select a depolarizing diffuser. A depolarizing diffuser will reflect half the flow-passage illumination with the correct polarization for recording a hologram. The diffuser reflection with the other polarization and the specular reflections contribute to the overall exposure level of the emulsion, but do not form a hologram with the reference wave. If the laser radiates enough energy per pulse, the measured beam ratio can be reduced to compensate for the reduction in image brightness, since less than half the object illumination produces a hologram. If the contribution of the object illumination to the average exposure is neglected, then the reduction in ratio is approximately the fraction of the total object beam that has the polarization of the reference beam. For example, if 33 percent of the object illumination has this polarization, then a measured beam ratio of 12 might be reduced to 4. The precisely calculated reduction would be less. A precise calculation involves summing two interference patterns. One pattern is formed between the useful diffuser reflection and the reference beam. The other pattern is formed between the remainder of the diffuser wave and the window reflection. Both patterns involve the laser speckle effect. For the example, a beam ratio between 6 and 8 would probably be a better choice.

When polarization rotation is used to eliminate the specular reflections from the reconstructed image, a well-polarized laser and precise control of the polarizations of the object and reference waves are required. The polarization of a beam can be rotated accidentally or intentionally by reflections and by optically active materials. Perfectly polarized beams cannot be created, so there always will be a residual image of the window reflection. Hence, it is recommended that polarization rotation be combined with collimation to minimize the effects of the specular reflections.

Note that the polarization of a laser beam is generally not uniform over the beam. At first glance, this is not a serious problem. The reference beam can be generated from a small segment of the laser-beam cross section. The reference beam will have nearly uniform polarization. If a depolarizing diffuser is used, the polarization of the object beam is not important. (This is another argument for using a depolarizing diffuser.) But for careful minimization of the specular reflections in the reconstructed image, ray-for-ray matching of the polarizations of the window-reflected and reference waves would be required.

Besides polarization, there are two other laser specifications of holographic significance: coherence and beam uniformity. Recall that a number of defects in the holographic process mimic the effects of small coherence. These effects include depolarization, large beam ratio, incorrect exposure and processing, emulsion shrinkage, and a reduction in the useful dynamic range due to noise waves. Even if the coherence is low, holocameras have been used to compensate (refs. 2 and 3). An adjustment of the beam ratio provides some compensation (eq. (13)). Still, it is desirable to record a uniformly bright image of the largest object of interest, without the need for holocamera path matching. The required coherence is determined from the maximum expected reference-ray, object-ray path difference. A useful specification for a pulsed laser is the spectroscopic line width. The reciprocal of this line width in inverse centimeters should exceed the maximum expected path difference.

An implicit assumption in specifying coherence is that there is enough energy in the laser pulse to take advantage of the specified coherence. Increasing the coherence permits larger objects to be recorded, and that requires more energy for the same beam ratio. The first version of the Nd:YAG laser had a coherence length of about a meter. But the 10-mJ/pulse was not enough to take advantage of the coherence length. The second version of the laser, at 50- to 100-mJ/double pulse, is better matched to its coherence length of about 30 cm.

Uniform and efficient illumination of the scene, without spatial filtering (an inconvenient process with a pulsed laser), requires a laser beam with a smooth profile. If the reference beam is not uniform, the beam ratio and efficiency at the hologram will change from point to point on the hologram. The first version of the Nd:YAG laser had the smooth beam profile associated with a TEM_{00} oscillator. The second version, using the unstable resonator, had a much less uniform profile. Because the profile was not smooth, it was necessary to derive both the object and reference waves from parts of their respective beams. The beams were diverged more than would have been necessary with a uniform beam, and the uniform portions were selected. Hence, the energy was not used efficiently, making the effective energy of the laser less than measured.

Once specular reflections are eliminated and a coherent, smooth laser beam is selected, the signal-to-noise can be kept high by satisfying the off-axis-reference-wave criterion, by selecting the right beam ratio and exposure, and by minimizing scattering. Although a low-brightness hologram with a high signal-to-noise ratio can be tolerated, the signal-to-noise will decrease due to scattering as the brightness of the image decreases. Scattering will be less for a red laser line than for the 532 nm line of the doubled Nd:YAG laser. Also, the Kodak SO 253 emulsion is more sensitive in the range of 610 to 640 nm.

Especially clean images of noise-wave-free subjects can be recorded by using unbleached holograms. A signal-to-noise approaching 100 is possible. Both scattering and nonlinear noise are less, when the hologram is not bleached. However, the holographic process must be controlled very well. Undesirable reflections must be eliminated. Development must be prompt. The performance of the laser must be predictable and constant.

For double-exposure interferometry, it is especially important that the properties of the laser beam not change between pulses of a pulse pair. More than a 20 percent fluctuation in the ratio between the intensities of the reconstructed object waves was undesirable. Hence, the energy of the pulses within a pulse pair should not differ by more than 10 percent. Also, the beam profiles of the pulses within a pulse pair should not differ. Otherwise, the fringe contrast and signal-to-noise will be unacceptably low.

A user of holographic interferometry will have less control over the interferometric process than over the holographic process. From the literature and from the section on localization and feature interferences, it can be concluded that the best subject for three-dimensional visualization will be isolated and have a small depth of field. But the depth of field can be used as a diagnostic tool, even when it is not small. The estimated depth-of-field for the boundary-layer turbulence exceeded the width of the flow passage. Some of the turbulence is indeed poorly localized in the reconstructed images, but some of the smaller, turbulent-like structure is well localized. Being able to characterize a structure as poorly or well localized places limits on its scale and density change.

It was pointed out that it may be profitable to avoid the introduction of extraneous fringes or the reduction of fringe contrast by recording holograms only during low velocity conditions of the diffuser and window.

Conclusions and Concluding Remarks

The program to use Nd:YAG lasers for holographic cinematography was originated in an effort to increase the hologram recording rate for flow visualization. To define a laser suitable for this application, it is necessary to be involved with three other areas of technology. These areas are holography in a wind tunnel, diffuse-illumination interferometry, and the properties of a flow. Some definite conclusions can be stated for the involvement of these component technologies, as well as for the selection of a laser.

Useful results can be obtained with a variety of approaches to the design of the Nd:YAG laser. The commercially available Nd:YAG laser continues to be improved by the manufacturers. At the time that this program was begun, 20 pulses per second was considered to be a high repetition rate. Now, 30-pulse-per-second lasers are readily available, and 50 pulses per second is considered to a be high repetition rate. Still, some general specifications for the design of an optimum laser can be concluded from this study, for objects in the size-range treated in this report.

A suitable Nd:YAG laser, producing around 100 mJ of 532-nm light per double pulse, should have a spectroscopic line width between 0.03 and 0.01 cm^{-1}. To fully use energies of a joule or more, the line width would be reduced to between 0.01 and 0.001 cm^{-1}. Energies higher than 100 mJ may be useful, even at the larger line widths, since a reflective diffuser can be very inefficient.

A smooth beam profile is necessary, if the energy of the laser is to be used efficiently. It is also essential that the properties of the laser beam not change between pulses of a pulse pair. To achieve these objectives simultaneously, the laser should consist of a low-energy TEM_{00} oscillator coupled with high amplification. With presently available laser rods, this design unfortunately requires two amplifiers. The development of a commercially available slab-YAG amplifier would eliminate the need for two amplifiers. Although not specifically discussed in this report, the reliability, ease of operation, the resistance to vibrational misalignment of the laser are also important in a wind-tunnel environment.

A laser can be used efficiently only if the fundamentals for making good holograms can be adhered to. These fundamentals include having the correct exposure, correct beam ratio, correct beam angles, correct development procedure, and a scene consisting only of the object of interest, free from extraneous reflections. A way usually can be found to observe the fundamentals using currently available lasers. Generating fringe patterns with a contrast factor around 20 is the objective. High-contrast fringe patterns are desirable for automated fringe-pattern analysis as well as for visualization.

The performance of the diffuse-illumination method for flow visualization depends strongly on the properties of the flow field. It is to be emphasized that the observed performance of diffuse-illumination interferometry is a diagnostic of the general properties of the flow field. The roughest models of the flow features can be used to estimate the scene depth. The observed scene depth can be compared with the estimate. It is expected that as holography is used more quantitatively for the measurement of flow properties in the future, flow modeling and the design and use of holographic instrumentation will become intimately connected.

The development of hardware for the entire holographic process should continue and should include improving the reliability and performance of the lasers as well as increasing the hologram repetition rate. New laser technologies must be evaluated for their suitability for holography as well as for the special advantages that they may offer. Evaluation of time-average, diffuse-illumination holographic interferometry as a flow visualization and measurement method should be pursued. A flashlamp-pumped dye laser can be used to generate pulses of the order of 10 μsec for time-average holography of flows such as those found in a flutter cascade. Time-average holography can be used to control the contrast of the fringe

associated with a selected flow feature. The contrast of that feature can be enhanced, and the signal-to-noise ratio of its reconstructed image increased.

Finally, the development of holographic flow visualization should be combined with the development of methods of the quantitiative analysis of holographic results. Automated fringe-measurement methods such as electronic heterodyne holographic interferometry also are being investigated.

Appendix—Symbols

A constant term in eq. (3) relating amplitude transmittance of hologram to exposure

A' $\exp(jFA + jfE_0/2)$

a x-distance moved by flow feature between exposures of a double-exposure hologram, m

B proportionality factor in eq. (1) where amplitude transmittance of hologram is proportional to recording intensity, m^2/V^2

B' factor in eq. (3) expressing amplitude transmittance of hologram as linear function of exposure, $m^2/V^2\,s$

b beam parameter for Gaussian beam, m

C coefficient of second order term in eq. (10) relating amplitude transmittance to intensity, m^4/V^4

$\mathcal{C}$ contrast

C' coefficient of second order term in expressions relating amplitude transmittance to exposure, $m^4/V^4\,s^2$

D holographic scene depth, m

E_0 average exposure of hologram, $V^2/m^2 s$

$\mathbf{E_o}$ time-independent electric-field vector of object wave, V/m

$\mathbf{E_r}$ time-independent electric-field vector of reference wave, V/m

F proportionality factor in eq. (23) relating phase modulation of a phase hologram to amplitude transmittance of original exposure, also F number

F_x,F_y spatial frequencies in x and y directions, m^{-1}

f $-2FB'$, $m^2/V^2 s$

$\mathcal{f}$ change in refractive index

G Glastone-Dale coefficient, m^3/kg

g proportionality factor in eq. (18), m^3

g' proportionality factor in eq. (19), m^3

h impulse response function (e.g., $h(\mathbf{r_h},\mathbf{r_d})$ and $h(\mathbf{r_h},\mathbf{r_d},t)$) m^{-2} or $m^2\,s^{-1}$

I interference pattern as in eq. (32); I is proportional to intensity, where proportionality constants are often ignored in practice, V^2/m^2

J_n Bessel function of first kind and order n

j $\sqrt{-1}$

K proportionality factor in eq. (34) relating interferometric phase to integral of density change, rad m^2/kg

k $2\pi/\lambda$, rad/m

L luminance, cd/m^2

Δl optical path-length difference, m

$N(x,y)$ noise along light ray, parameterized with intersection coordinates x,y in diffuser plane, V^2/m^4

O phasor representing scalar object wave, V/m

$\bar{O}$ phasor representing time-averaged scalar object wave, V/m

O_i information part of scalar object wave, V/m

O_n noise part of scalar object wave, V/m

O_1,O_2 phasors representing scalar object waves at exposures 1 and 2 of double-exposure hologram, V/m

P ratio of reference-wave intensity to object-wave intensity

R phasor representing reference wave, V/m

r position vector or radial distance from center of eddy, m

$\mathbf{r_d}$ position vector of point on diffuser, m

$\mathbf{r_h}$ position vector of point on hologram, m

$\mathbf{r_i}$ position vector of point in image, m

r_0 radius of eddy, m

$|S|$ $|B'|/2$, $V^2/m^2 s$

T amplitude or field transmittance of hologram

T' amplitude or field transmittance of bleached hologram

t_e exposure time, s

U_i magnitude of information part of object wave, V/m

U_n magnitude of noise part of object wave, V/m

U_o magnitude of object-wave phasor, V/m

U_1,U_2 magnitudes of object wave at first and second exposures of double-exposure hologram, V/m^2

U_r magnitude of scalar reference-wave phasor, V/m

V fringe visibility or, simply, visibility

v time rate of change of path length, m/s

W Gaussian-beam waist, m

x,y rectangular coordinates in hologram plane or in diffuser plane, m

$\Delta x,\Delta y$ half projections on diffuser of light-ray pencil, m

x_0,y_0 coordinate of intersection of viewing axis with diffuser plane, m

Z z-coordinate of point of localization measured from diffuser plane, m

Z_H distance between virtual image of object-illumination source and hologram, m

Z_0 z-coordinate of center of eddy measured from diffuser plane, m

z z-coordinate, m

γ localization coefficient, eq. (46)

Δ denotes difference or depth of field, m

δ displacement of diffuser, m

2δ length of light-ray segment intersecting eddy, m

$\delta(x)$ Dirac delta function of argument x, m^{-1}

η efficiency of hologram

θ shock-wave angle relative to x-axis, deg

θ_o half angle of field of view of object wave at hologram, deg

θ_r angle between object-wave axis and reference-wave axis, deg

$\theta_x\theta_y$ angular variations relative to viewing axis; variations are directed along x and y directions in diffuser plane, deg

λ wavelength of light, nm

μ complex degree of temporal coherence, or coefficient for reduction of fringe visibility due to decorrelation

$|\mu_v|^2$ coefficient for reduction of image brightness due to object motion

ρ fluid density or radial coordinate, kg/m^3 or m

ρ_0 reference density or maximum density in eddy, kg/m^3

$\Delta\rho(r)$ change in density as a function of position, kg/m^3

ρ_s change in density across shock wave, kg/m^3

$\Delta\varphi$ interferometric phase or phase change, rad

φ_i phase of information part of object-wave phasor, rad

φ_n phase of noise part of object-wave phasor, rad

φ_o phase of object-wave phasor, rad

φ_r phase of reference-wave phasor, rad

ψ depolarization coefficient; $\sqrt{\psi}$ is cosine of angle between object-wave and reference-wave polarizations

References

1. Witte, A.B.; and Wuerker, R.F.: Laser Holographic Interferometry Study of High Speed Flow Fields. AIAA Paper 69-347, Apr. 1969.
2. Wuerker, R.F.; et al.: Application of Holography to Flow Visualization Within Rotating Compressor Blade Row. (AIRESEARCH-73-9489, AiResearch Mfg. Co.; NASA Contract NAS3-15336.) NASA CR-121264, 1974.
3. Decker, A.J.: Fringe Localization Requirements for Three-Dimensional Flow Visualization of Shock Waves in Diffuse-Illumination, Double-Pulse Holographic Interferometry. NASA TP-1868, 1982.
4. Decker, A.J.: Holographic Flow Visualization of Time Varying Shock Waves. Appl. Opt., vol. 20, no. 18, Sept. 15, 1981, pp. 3120-3127.
5. Klauminzer, G.K.: Twenty Years of Commerical Lasers—A Capsule History. Laser Focus/Electro-Optics, vol. 20, no. 12, Dec. 1984, pp. 54-79.
6. Hall, R.J.; and Eckbreth, A.G.: Flame Diagnosis by Coherent Anti-Stokes Raman Spectroscopy. Laser Spectroscopy—Applications and Techniques, SPIE Proc., vol. 158, SPIE, 1978, pp. 59-73.
7. Eckbreth, A.C.; et al.: CARS Temperature and Species Measurements in Augmented Jet Engine Exhausts. Appl. Opt., vol. 23, no. 9, May 1, 1984, pp. 1328-1339.
8. Rahn, L.A.; and Mattern, P.L.: Coherent Raman Spectroscopy for Combustion Applications. Laser Spectroscopy—Applications and Techniques, SPIE Proc., vol. 158, SPIE, 1978, pp. 76-83.
9. Koechner, W.: Solid-State Laser Engineering. Springer-Verlag, 1976.
10. Decker, A.J.: Holographic Cinematography of Time-Varying Reflecting and Time-Varying Phase Objects Using a Nd:YAG Laser. Opt. Lett., vol. 7, no. 3, Mar. 1982, pp. 122-123.
11. Boldman, D.R.; and Buggele, A.E.: Wind Tunnel Tests of a Blade Subjected to Midchord Torsional Oscillation at High Subsonic Stall Flutter Conditions. NASA TM-78998, 1978.
12. Boldman, D.R.; Buggele, A.E.; and Decker, A.J.: Three-Dimensional Shock Structure in a Transonic Flutter Cascade. AIAA J., vol. 20, no. 8, Aug. 1982, pp. 1146-1148.
13. Decker, A.J.: Holographic Cinematography and Other Dynamic Flow Visualization Methods. Flow Visualization and Laser Velocimetry for Wind Tunnels. NASA CP-2243, W.W. Hunter, Jr. and J.T. Foughner, Jr., eds., 1982, pp. 175-177.
14. Decker, A.J.: Measurement of Fluid Properties Using Rapid-Double-Exposure and Time-Average Holographic Interferometry. AIAA Paper 84-1461, June 1984.
15. Ebert, J.; and Eberhard, K.: Measurement of Laser-Induced Damage With an Unstable Resontor-Type Laser. Appl. Opt., vol. 23, no. 21, Nov. 1, 1984, pp. 3759-3761.
16. Boldman, D.R.; Buggele, A.E.; and Michalson, G.M.: Stall Flutter Experiment in a Transonic Oscillating Linear Cascade. NASA TM-82655, 1981.
17. Collier, R.J.; Burckhardt, C.B.; and Lin, L.H.: Optical Holography. Academic Press, 1971.
18. Caulfield, H.J., ed.: Handbook of Optical Holography. Academic Press, 1979.
19. Abramson, N.H.: The Making and Evaluation of Holograms. Academic Press, 1981.
20. Stroke, G.W.: An Introduction to Coherent Optics and Holography. 2nd ed., Academic Press, 1969.
21. Jones, R.; and Wykes, C.: Holographic and Speckle Interferometry. Cambridge University Press, 1983.
22. Sobolev, G.A., ed.: Recording Materials for Holographic Imaging and Cine-holography. Izdatel'stvo Nauka, Leningrad, 1979 (In Russian).
23. Landry, M.J.; and Phipps, G.S.: Holographic Characteristics of 10E75 Plates for Single- and Multiple-Exposure Holograms, Appl. Oct., vol. 14, no. 9, Sept. 1975, pp. 2260-2266.
24. Decker, A.J.: Holography Through Optically Active Windows. NASA TP-1414, 1979.
25. Goodman J.W.: Introduction to Fourier Optics. McGraw-Hill, 1968.
26. Abramowitz, M.; and Stegun, I.A.: Handbook of Mathematical Functions. Dover, 1965, p. 361.
27. Vest, C.M.: Holographic Interferometry. Wiley, 1979.
28. Schumann, W.: Fringe Localization in Holographic Interferometry in the Case of a Transparent Object with a Nonuniformly Varying Index of Refraction. Opt. Lett., vol. 7, no. 3, Mar. 1982, pp. 119-121.
29. Fry, G.A.: The Eye and Vision. Applied Optics and Optical Engineering. Vol. 2—The Detection of Light and Infrared Radiation, R. Kingslake, ed., Academic Press, 1965, pp. 1-76.

1. Report No.	2. Government Accession No.	3. Recipient's Catalog No.
NASA TP-2593		

4. Title and Subtitle	5. Report Date
Evaluation of Diffuse-Illumination Holographic Cinematography in a Flutter Cascade	July 1986
	6. Performing Organization Code: 505-62-0
7. Author(s): Arthur J. Decker	8. Performing Organization Report No.: E-2937
	10. Work Unit No.
9. Performing Organization Name and Address: National Aeronautics and Space Administration, Lewis Research Center, Cleveland, Ohio 44135	11. Contract or Grant No.
	13. Type of Report and Period Covered: Technical Paper
12. Sponsoring Agency Name and Address: National Aeronautics and Space Administration, Washington, D.C. 20546	14. Sponsoring Agency Code

15. Supplementary Notes

16. Abstract

Since 1979, the Lewis Research Center has conducted an investigation of the use of holographic cinematography for three-dimensional flow visualization. The lasers used were Q-switched, double-pulse, frequency-doubled Nd:YAG lasers, operating at 20 double pulses per second. The primary subjects for flow visualization were the shock waves produced in two flutter cascades. The flow visualization was obtained by diffuse-illumination, double-exposure, holographic interferometry. This report is an evaluation of the performances of the Nd:YAG lasers, of holography, and of diffuse-illumination interferometry in the single-window wind tunnels used for this investigation. The fringe-contrast factor is used to evaluate the results. The effects of turbulence on shock-wave visualization in a transonic flow are discussed. The depth of field for visualization of a turbulent structure is demonstrated to be a measure of the relative density and scale of that structure. Other items discussed in detail are the holographic emulsion, tests of coherence and polarization, effects of windows and diffusers, hologram bleaching, laser configurations, influence and handling of specular reflections, modes of fringe localization, noise sources, and coherence requirements as a function of the pulse energy. Also, holography and diffuse illumination interferometry are reviewed.

17. Key Words (Suggested by Author(s))	18. Distribution Statement
Holography; Holographic interferometry; Holographic cinematography; Neodymium lasers; Flow visualization; Cascade wind tunnels; Flutter	Unclassified – unlimited STAR Category 35

19. Security Classif. (of this report)	20. Security Classif. (of this page)	21. No of pages	22. Price*
Unclassified	Unclassified	34	A03

*For sale by the National Technical Information Service, Springfield, Virginia 22161

NASA-Langley, 1986